Szabolcs Berezvai

Final Project

Budapest University of Technology and Economics
Faculty of Mechanical Engineering
Department of Applied Mechanics

# Final Projects

MŰEGYETEM 1782


Budapest University of Technology and Economics

Faculty of Mechanical Engineering

Department of Applied Mechanics


**Szabolcs BEREZVAI**

# Visco-hyperelastic characterization of polymeric foams

Final Project

Supervisor: Dr. Attila KOSSA, assistant professor
Department of Applied Mechanics

Budapest, 2015

# Declarations

*Declaration of acceptance*

This thesis fulfils all formal and content requirements prescribed by the Faculty of Mechanical Engineering of Budapest University of Technology and Economics, as well as it fully complies all tasks specified in the transcript. I consider this thesis as it is suitable for submission for public review and for public presentation.

Done at Budapest, 11.12.2015

*dr. Attila Kossa*

*Declaration of independent work*

I, Szabolcs Berezvai, the undersigned, hereby declare that the present thesis work has been prepared by myself without any unauthorized help or assistance such that only the specified sources (references, tools, etc.) were used. All parts taken from other sources word by word or after rephrasing but with identical meaning were unambiguously identified with explicit reference to the sources utilized.

*Szabolcs Berezvai*

*Declaration of authorization*

I authorize the Faculty of Mechanical Engineering of the Budapest University of Technology and Economics to publish the principal data of the thesis work (author's name, title, abstracts in English and in Hungarian, year of preparation, supervisor's name, etc.) in a searchable, public, electronic and online database and to publish the full text of the thesis work on the internal network of the university (or for authenticated users). I declare that the submitted hard copy of the thesis work and its electronic version are identical. Full text of thesis works classified upon the decision of the Dean will be published after two years.

Done at Budapest, 11.12.2015

*Szabolcs Berezvai*

# Acknowledgements

First of all, I would like to express my deepest thanks to my supervisor, dr. Attila KOSSA assistant professor (Department of Applied Mechanics) for his outstanding guidance and constant support during my work. I am indebted for all the invaluable support and inspiration he gave me during our common work in the last years. I am also grateful that he endeared to me the mechanics of polymer foams and introduced me the beauty of researchers' life.

I got insights into the manufacturing technology of polyer foams during my summer internship at Furukawa Electric Institute of Technology (FETI Kft). These experiences were beneficial for my thesis.

I would like to thank my friends, mates and my family, who I could always count on indeed. Especially to my Mum, who always supported my dreams and goals.

This research has been supported by the Hungarian Scientific Research Fund, Hungary (Project Identifier: PD 108691) and the National Talent Programme of the Hungarian Government (Contract Identifier: NTP-EF-P-15-0085), which are gratefully acknowledged.

# Abstract

Keywords: *viscoelasticity, hyperelasticity, parameter fitting, finite strain theory, polymer foams*

Polymer foams are widely applied cellular materials due to their mechanical behaviour and high energy absorption properties. The deformations of polymer foams can be characterised by large strains (in case of volumetric compression) and large displacements, which shows visco-elastic material behaviour. The main field of application is packaging and impact protection, but polymer foams appear in everyday use like as ear-plugs and memory foams as well.

The behaviour of large elastic and viscoelastic materials can be described by the so-called visco-hyperelastic material model, which combines the hyperelastic and the viscoelastic material models. In this approach the time-dependent stress-relaxation phenomenon is modelled using Prony-series representation, while for the long-term time-independent behaviour hyperelastic material model is proposed, which can be derived from the corresponding strain energy function.

In this thesis I investigate the modelling of the visco-hyperelastic material behaviour in case of homogeneous deformations of a particular memory foam material applied in mattresses. The most widely used compressible hyperelastic material model, the Ogden-Hill model and the finite strain viscoelastic constitutive law implemented in the commercial finite element software ABAQUS are also provided. Using these models the closed-form stress response functions were determined in case of homogeneous deformations. This provided closed-form solutions, which are not available in the literature yet, enables us to obtain material parameters directly from the experimental data using parameter-fitting.

The usual algorithm of parameter-fitting is to separate the parameter-fitting of the long-term behaviour and the parameter-fitting of the stress relaxation. In this approach it is assumed that the stress-relaxation is investigated in case of step load. However, in case of real measurements only ramp loading can be performed, which leads to errors in the relaxation test data. The analytically determined stress response yields that the entire visco-hyperelastic model can be fitted to the real measurement data in case of ramp test. Using this latter method more accurate material parameters can be provided for the investigated memory foam material. Finally, the fitted model was investigated in Abaqus in order to analyse the numerical behaviour of the model and to compare it with the measured data.

# Contents

# 1 Introduction

## 1.1 Polymer foams and their application

Polymer foams are widely applied cellular materials, thanks to their favourable mechanical behaviour and high energy absorption properties. Due to their cellular structure, polymer foams are light-weight with low overall density since they are typically 90% space. Additionally, the mechanical behaviour is characterised by low moduli, such as the elastic modulus, the shear modulus and the bulk modulus. The deformation of polymer foams also exhibits large deformations and displacements. These properties might suggest that polymer foams are of little use from the industrial point of view. However, in the field of impact protecting and packaging we require materials with high energy absorption properties and low stiffness and strength that can be controlled easily during the manufacturing process. Polymer foams provide these requirements [1].

Thanks to the above mentioned properties, polymer foams are applied mostly in the industrial field of impact protecting and packaging. The primary goal here is to protect the products from impacts and damages during transportation, storage and delivery, and additionally to damp the environmental vibrations and insulate the product. Beside the industrial applications, polymer foams can be familiar from everyday life like sport shoe treads, mattresses, car seats, helmets or ear plugs. In these applications the most important function is to protect, support and insulate the human body. An inproper support of the body during sleeping, sitting and running may cause serious orthopaedic problems and may increase the risk of thrombosis [2].

Beside the large energy absorption property, the mechanical behaviour of polymer foams shows time-dependent, i.e. viscoelastic properties. The viscoelastic property means, that the mechanical behaviour of the polymer foams are not only affected by the load but also by the loading rate. The most significant viscoelastic phenomena are the stress relaxation and the creep. In order to analyse properly the mechanical behaviour of such a viscoelastic material, the time-history of the loading is required to be obtained precisely, which encumbers the design process. These viscoelastic properties are utilized for instance in car seats, which should support the driver and also damp out the vibrations caused by rough road surfaces [3].

These time-dependent properties are presented also in the memory foam layers of mattresses, where the length of the loading, caused by the human body during the sleep, is several hours. The memory foams were developed by NASA for spaceship seats. After the first experiments the results were published for public domain. The first commercial memory foam mattress was released by the Swedish Fagerdala World Foams in 1991. Since then, several manufacturers have joined into the production and development. The memory foam mattresses, due to their viscoelastic properties, are able to follow the body shape, thus supporting the body uniformly (see Fig. 1.1). Therefore, the pressure on the backbone and the body decreases, which makes the sleep more comfortable and deeper [4].

a) b)

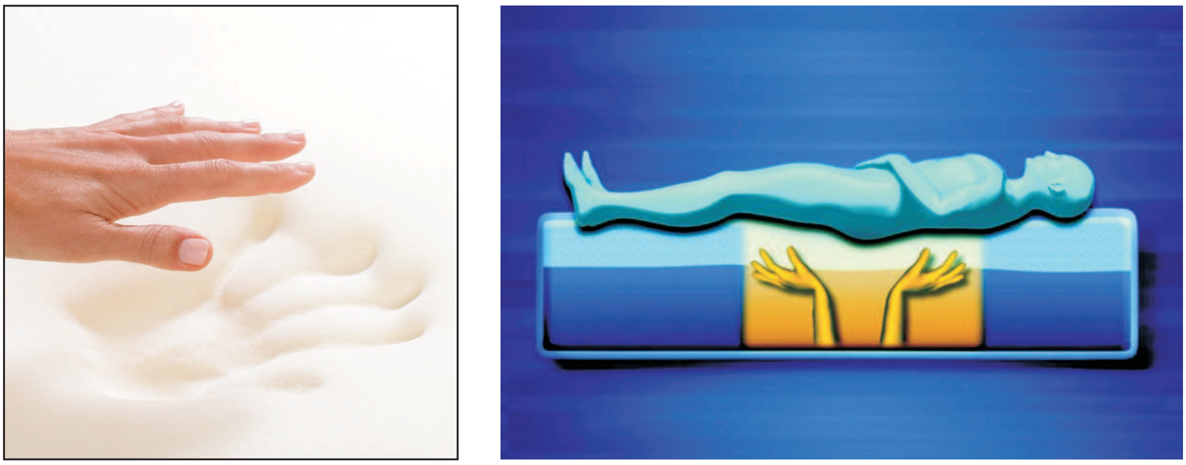

**Figure 1.1:** The commercial a) memory foams and b) the body shape following support of memory foam mattresses Sources: cardo.hu, matracguru.hu

## 1.2 Aim of the work

Since polymer foams are widely applied materials, there is a significant need to understand and model their mechanical behaviour properly in order to improve the finite element analysis of such materials. The behaviour of large elastic and viscoelastic materials can be described using the so-called visco-hyperelastic constitutive equation, which combines the hyperelastic and the viscoelastic material models. This modelling approach can describe the mechanical behaviour with adequate precision. These complex material models are available in all commercial finite element software including Abaqus [5]. In this approach the time-dependent stress-relaxation phenomenon is modelled using the Prony-series representation, while for the long term time-independent behaviour a hyperelastic material model is adopted, which can be derived from the corresponding strain energy function.

The goal of the thesis is to investigate the visco-hyperelastic material modelling approach applied for a particular polyurethane foam material in memory foam layer of a commercial mattress. Additionally, based on this material model, the closed-form stress solutions are also to be derived in case of some homogeneous deformations, which enables us to obtain the material parameters directly from experimental data using a parameter-fitting algorithm. The usually adopted algorithm to find the material parameters for a particular material is to separate the parameter-fitting of the long-term behaviour and the stress relaxation. This approach induces significant errors into the fitting process, consequently the fitted material parameters cannot describe accurately the overall visco-hyperelastic behaviour and the solution will be inaccurate [6],[7]. Using the analytically derived stress-response functions, which have not been provided in the literature yet, the entire visco-hyperelastic material model can be fitted to the measurement data in one step [8]. Therefore the fitted parameters will be more accurate, especially in the relaxation region.

The main motivation of my work was the possibility that in case of open-cell polymer foams (like the investigated memory foam), the stress-response functions can be expressed in closed-form for homogeneous loads [9], [10]. This closed-form solutions are not available in the literature yet, thus this is a novel method to provide a more accurate modelling approach for polymer foams. The advantages of the closed-form parameter fitting process are presented in Fig. 1.2. The further details on the parameter fitting process are discussed later in *Chapter 6*.

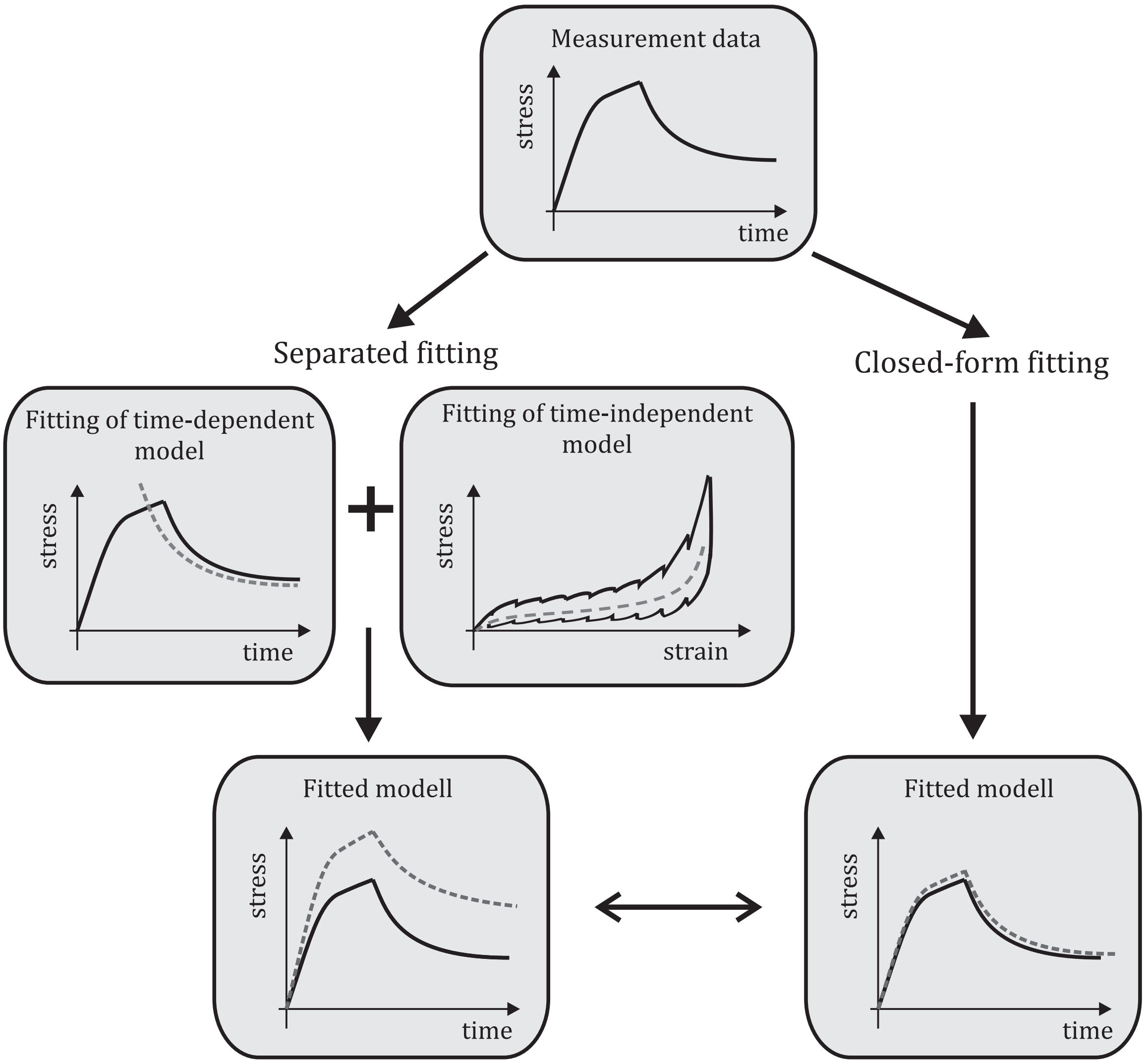


**Figure 1.2:** The advantages of closed-cell fitting - the main motivation of the thesis

## 1.3 Outline of the thesis

The thesis contains 6 chapters. The first chapter (*Chapter 1*) contains a general introduction into the properties and applications of polymer foams. Then, the goals and the structure of the thesis are reviewed and finally, the most important notations are summarized.

In *Chapter 2*, the hyperelastic material models are introduced, including the most widely applied Ogden–Hill's compressible hyperelastic material model. Some details about its history are also provided in this chapter. Finally, the stability of the material model is discussed.

*Chapter 3* provides an overview on the mechanical properties of the rate-dependent materials and summarizes the viscoelastic modelling approaches using the formalism available in Abaqus [5]. Firstly, the linear viscoelastic material model introduced, from which the finite strain visco-hyperelastic material model can be derived. This chapter also includes a possible numerical integration algorithm for stress response using the large strain visco-hyperelastic material model.

In *Chapter 4*, the closed-form stress response solutions are derived and summarized in case of homogeneous deformations, namely uniaxial, equibiaxial and volumetric compression. Besides, the stress solutions using the new formulation in Abaqus [5] are also presented.

*Chapter 5* provides the measurements performed on a particular open-cell polyurethane foam material,which applied in the memory foam layer of commercial mattresses. In this chapter the measurement layout, the specimens, the process of evaluation and the measurement result are also presented.

In *Chapter 6*, the material parameter fitting process is discussed. Two parameter fitting approaches were applied to determine the material parameters in the visco-hyperelastic material model based on the measurement data. The fitted parameters are provided for the separated and the closed-form fitting methods as well. Finally, the performances of the fitted models are compared using finite element analysis and predictions for some further loading cases are presented.

In the end, *Chapter 7* summarizes the main results of the thesis both in English and Hungarian. The thesis includes *Appendices* as well. In *Appendix A* the relation of the Ogden–Hill's material model and the Hooke's law is discussed, in *Appendix B* the numerical implementation of the visco-hyperelastic material model is presented, while in *Appendix C* the incomplete gamma function and its properties are summarized.

## 1.4 Nomenclature

**Latin letters**

| | |
|---|---|
| $A_0$ | Initial cross section |
| $\boldsymbol{b}$ | Left Cauchy–Green deformation tensor |
| $\boldsymbol{C}$ | Right Cauchy–Green deformation tensor |
| $E$ | Elastic modulus (Young's modulus) |
| $e_k$ | Relative elastic modulus |
| $\mathbf{E}_1, \mathbf{E}_2, \mathbf{E}_3$ | Unit basis vectors in the reference configuration |
| $\mathbf{e}_1, \mathbf{e}_2, \mathbf{e}_3$ | Unit basis vectors in the spatial configuration |
| $\boldsymbol{F}$ | Deformation gradient |
| $F$ | Load, force |
| $G$ | Shear modulus |
| $g_i$ | Relative shear modulus |
| $H_0$ | Initial separation |
| $\boldsymbol{I}$ | Second-order identity tensor |
| $I_1, I_2, I_3$ | Scalar invariants of $\boldsymbol{C}$ and $\boldsymbol{b}$ |
| $J$ | Volume ratio (determinant of $\boldsymbol{F}$) |
| $K$ | Bulk modulus |
| $k_i$ | Relative bulk modulus |
| $L_0$ | Height of the specimen |
| $\boldsymbol{n}^{(a)}$ | Unit eigenvectors of $\boldsymbol{b}$ |
| $\boldsymbol{N}^{(a)}$ | Unit eigenvectors of $\boldsymbol{C}$ |
| $N$ | Order of the hyperelastic material model |
| $P$ | Order of the Prony-series |
| $\boldsymbol{P}$ | 1st Piola–Kirchhoff stress tensor |
| $\boldsymbol{S}$ | 2nd Piola–Kirchhoff stress tensor |
| $W$ | Strain energy function |

**Greek letters**

| | |
|---|---|
| $\alpha_i,\ \beta_i,\ \mu_i$ | Material parameters in the Ogden–Hill's hyperelastic material model |
| $\Gamma(\nu, x)$ | Upper incomplete gamma function |
| $\delta$ | Relative error |
| $\varepsilon$ | Engineering strain |
| $\dot{\varepsilon}$ | Engineering strain rate |
| $\lambda$ | Stretch |
| $\nu$ | Poisson's ratio |
| $\sigma$ | Cauchy stress |
| $\boldsymbol{\sigma}$ | Cauchy stress tensor |
| $\tau$ | Krichhoff stress |
| $\boldsymbol{\tau}$ | Krichhoff stress tensor |
| $\tau_i$ | Prony parameters |

# 2

# Hyperelastic modelling of polymer foams

The following theoretical summary is based on the books of I. Dorghi (2000) [11], A. Bower (2010) [12], and E. A. de Souza *et al.* (2008) [13].

The deformation of polymer foams shows viscoelastic behaviour, which means that after the removal of the applied load the body gradually retrieves its original shape. Since these time-dependent (or rate-dependent) deformations are characterised by large strains and large displacements, the so-called visco-hyperelastic modelling approach is used. Such material models are consists of two parts: a hyperelastic and a viscoelastic model. In this approach the viscoelastic model characterises the relaxation, while the hyperelastic model describes the nonlinear finite strain elastic behaviour. Therefore, in order to understand better the behaviour of visco-hyperelastic material models, the time-independent hyperelastic material models corresponding to the long term and the instantaneous loads should be investigated first.

## 2.1 Theory of hyperelastic constitutive equations

In linear isotropic elasticity the stress and the strain are related by the Hooke's law as

$$\boldsymbol{\sigma} = \frac{E}{1+\upsilon}\left[\boldsymbol{\varepsilon} + \frac{\nu}{1-2\nu}\varepsilon_I \boldsymbol{I}\right]. \tag{2.1}$$

For simplicity, let us introduce the 4th-order elasticity tensor $\boldsymbol{\mathcal{D}}^e$ (also called as Hooke's operator), which is defined as

$$\boldsymbol{\mathcal{D}}^e = \frac{E}{1+\upsilon}\boldsymbol{\mathcal{T}} + \frac{\nu}{3\,(1-2\nu)}\boldsymbol{I} \otimes \boldsymbol{I}, \tag{2.2}$$

where $\boldsymbol{\mathcal{T}}$ is the 4th-order tensor representing the deviatoric projection. Therefore, the Hooke's law can be rewritten in a simplified form using the Hooke's operator as

$$\boldsymbol{\sigma} = \boldsymbol{\mathcal{D}}^e : \boldsymbol{\varepsilon}. \tag{2.3}$$

Alternatively, we can also express the linear stress-strain relation (i.e. the Hooke's law) as

$$\boldsymbol{\sigma} = \frac{\partial}{\partial \boldsymbol{\varepsilon}}\left(\frac{1}{2}\boldsymbol{\varepsilon} : \boldsymbol{\mathcal{D}}^e : \boldsymbol{\varepsilon}\right), \tag{2.4}$$

where the scalar-valued function $W(\boldsymbol{\varepsilon}) = \frac{1}{2}\boldsymbol{\varepsilon}\colon \boldsymbol{\mathcal{D}}^e\colon \boldsymbol{\varepsilon}$ is the stored elastic (or strain) energy per unit volume. This yields, that the stress tensor can be expressed as the partial derivative of the scalar function $W$ with respect to the strain tensor $\boldsymbol{\varepsilon}$ as

$$\boldsymbol{\sigma} = \frac{\partial W(\boldsymbol{\varepsilon})}{\partial \boldsymbol{\varepsilon}}. \tag{2.5}$$

Similarly, when the mechanical behaviour cannot be described using small-strain theory i.e. we consider nonlinear, finite-strain material response, the so-called hyperelastic constitutive equations can also be derived from a scalar function $W(\boldsymbol{F})$, which expresses the stored strain energy per unit reference volume in the function of deformation gradient $\boldsymbol{F}$, thus

$$W = W(\boldsymbol{F}). \tag{2.6}$$

Assuming that there exists of such a function $W(\boldsymbol{F})$ for a hyperelastic material leads that the stress power per unit reference volume is equal to the time derivative of $W(\boldsymbol{F})$ i.e. $\dot{W}$. The stress power $\dot{W}$ can also be related to the Cauchy stress tensor ($\boldsymbol{\sigma}$), the Kirchhoff stress tensor ($\boldsymbol{\tau}$) and the 1st Piola-Kirchhoff stress tensor ($\boldsymbol{P}$) as

$$\dot{W} = J\boldsymbol{\sigma} : \boldsymbol{d} = \boldsymbol{\tau} : \boldsymbol{d} = \boldsymbol{P} : \dot{\boldsymbol{F}}, \tag{2.7}$$

where $J = \det \boldsymbol{F}$ is the volume ratio and $\boldsymbol{d}$ the rate of deformation. Simultaneously, $\dot{W}$ can be expressed as the time derivative of the strain energy function $W(\boldsymbol{F})$ by applying the chain rule of derivation, therefore

$$\dot{W} = \frac{\partial W(\boldsymbol{F})}{\partial \boldsymbol{F}} : \dot{\boldsymbol{F}}. \tag{2.8}$$

Comparing the formulations of $\dot{W}$ in (2.7) and (2.8) we get

$$\boldsymbol{P} : \dot{\boldsymbol{F}} = \frac{\partial W(\boldsymbol{F})}{\partial \boldsymbol{F}} : \dot{\boldsymbol{F}}, \tag{2.9}$$

which yields that the 1st Piola–Kirchhoff stress tensor ($\boldsymbol{P}$) can be directly derived from the strain energy function as

$$\boldsymbol{P} = \frac{\partial W(\boldsymbol{F})}{\partial \boldsymbol{F}}. \tag{2.10}$$

When an additional rigid body rotation ($\boldsymbol{Q}$) added to the deformation, the deformation gradient satisfies the material objectivity, thus the modified deformation gradient becomes $\tilde{\boldsymbol{F}} = \boldsymbol{QF}$. This yields, that the strain energy function can be rewritten as

$$W(\boldsymbol{F}) = W(\boldsymbol{QF}), \tag{2.11}$$

because the stored strain energy does not change when an additional rigid body rotation is applied on the body. Additionally, the deformation gradient can be related to the right Cauchy–Green deformation tensor $\boldsymbol{C}$ using the spatial decomposition theorem as

$$\boldsymbol{F} = \boldsymbol{RU} = \boldsymbol{R}\sqrt{\mathbf{C}}. \tag{2.12}$$

If we choose the rigid body rotation according to $\boldsymbol{Q} = \boldsymbol{R}^T$, then $W$ can be expressed as the function of $\boldsymbol{U} = \sqrt{\mathbf{C}}$. Consequently, the strain energy function $W$ is also the function of the right Cauchy–Green deformation tensor $\mathbf{C}$, therefore

$$W(\boldsymbol{F}) = \tilde{W}(\boldsymbol{C}), \tag{2.13}$$

from which the stress power can be expressed as

$$\dot{W} = \frac{\partial W(\boldsymbol{F})}{\partial \boldsymbol{F}} : \dot{\boldsymbol{F}} = \frac{\partial \tilde{W}(\boldsymbol{C})}{\partial \boldsymbol{C}} \frac{\partial \boldsymbol{C}}{\partial \boldsymbol{F}} : \dot{\boldsymbol{F}}. \tag{2.14}$$

It is also known that $\boldsymbol{C} = \boldsymbol{F}^T\boldsymbol{F}$ is a symmetric tensor, therefore its partial derivative in (2.14) can be simplified as

$$\frac{\partial \boldsymbol{C}}{\partial \boldsymbol{F}} = 2\boldsymbol{F}. \tag{2.15}$$

Consequently, when the strain energy function $W$ is related to the right Cauchy–Green deformation tensor as $W = W(\mathbf{C})$, the 1st Piola–Kirchhoff stress tensor becomes

$$\boldsymbol{P} = 2\boldsymbol{F}\frac{\partial W(\boldsymbol{C})}{\partial \boldsymbol{C}}. \tag{2.16}$$

Therefore, applying the relations of the stress tensors, the 2nd Piola–Kirchhoff stress tensor ($\mathbf{S}$), the Kirchhoff stress tensor ($\boldsymbol{\tau}$) and the Cauchy stress tensor ($\boldsymbol{\sigma}$) can also be expressed using $W(\boldsymbol{C})$. Thus

$$\boldsymbol{S}{=}\boldsymbol{F}^{-1}\boldsymbol{P} = 2\frac{\partial W(\boldsymbol{C})}{\partial \boldsymbol{C}}, \tag{2.17}$$

$$\boldsymbol{\tau}{=}\boldsymbol{P}\boldsymbol{F}^T = 2\boldsymbol{F}\frac{\partial W(\boldsymbol{C})}{\partial \boldsymbol{C}}\boldsymbol{F}^T, \tag{2.18}$$

$$\boldsymbol{\sigma}{=}\frac{1}{J}\boldsymbol{P}\boldsymbol{F}^{\mathbf{T}} {=}\frac{2}{J}\boldsymbol{F}\frac{\partial W(\boldsymbol{C})}{\partial \boldsymbol{C}}\boldsymbol{F}^T. \tag{2.19}$$

In case of isotropic material the strain energy function $W(\boldsymbol{C})$ is either the function of the principal invariants of $\boldsymbol{C}$ ($I_1, I_2$ and $I_3$) or the principal stretches ($\lambda_1, \lambda_2$ and $\lambda_3$). Therefore

$$W = W(I_1, I_2, I_3) \quad \text{or} \quad W = W(\lambda_1, \lambda_2, \lambda_3), \tag{2.20}$$

where the scalar invariants of $\boldsymbol{C}$ are defined as

$$I_1 = \mathrm{tr}[\boldsymbol{C}], \qquad I_2 = \frac{1}{2}(I_1^2 - \mathrm{tr}[\boldsymbol{C}^2]), \qquad I_3 = \det \boldsymbol{C} = J^2. \tag{2.21}$$

Since the $(\lambda_i)^2$ are the eigenvalues of tensor $\boldsymbol{C}$, the scalar invariants can be expressed using the principal stretches ($\lambda_1, \lambda_2$ and $\lambda_3$) as

$$I_1 = \lambda_1^2 + \lambda_2^2 + \lambda_3^2, \qquad I_2 = (\lambda_1\lambda_2)^2 + (\lambda_1\lambda_3)^2 + (\lambda_2\lambda_3)^2, \qquad I_3 = (\lambda_1\lambda_2\lambda_3)^2. \tag{2.22}$$

Let's consider the case when the strain energy function is defined using the principal stretches, i.e. $W = W(\lambda_1, \lambda_2, \lambda_3)$. Then the chain-rule for derivation gives that

$$\boldsymbol{S}{=}2\frac{\partial W(\lambda_1, \lambda_2, \lambda_3)}{\partial \boldsymbol{C}} = 2\sum_{k=1}^{3}\frac{\partial W(\lambda_1, \lambda_2, \lambda_3)}{\partial \lambda_k}\frac{\partial \lambda_k}{\partial \boldsymbol{C}}, \tag{2.23}$$

where the corresponding derivation rule is

$$\frac{\partial \lambda_k}{\partial \boldsymbol{C}} = \frac{1}{2\lambda_k}\boldsymbol{N}^{(k)} \otimes \boldsymbol{N}^{(k)}, \tag{2.24}$$

in which $\boldsymbol{N}^{(k)}$ are the unit eigenvectors of $\boldsymbol{C}$. Then substituting (2.24) back into (2.23), the 2nd Piola-Kirchhoff stress tensor $\boldsymbol{S}$ becomes

$$\boldsymbol{S} = \sum_{k=1}^{3} \frac{1}{\lambda_k} \frac{\partial W}{\partial \lambda_k} \boldsymbol{N}^{(k)} \otimes \boldsymbol{N}^{(k)}. \tag{2.25}$$

Therefore, applying the relation of the stress tensors in (2.17)-(2.19), they can be expressed as

$$\boldsymbol{\sigma} = \sum_{k=1}^{3} \frac{\lambda_k}{J} \frac{\partial W}{\partial \lambda_k} \boldsymbol{n}^{(k)} \otimes \boldsymbol{n}^{(k)}, \tag{2.26}$$

$$\boldsymbol{\tau} = \sum_{k=1}^{3} \lambda_k \frac{\partial W}{\partial \lambda_k} \boldsymbol{n}^{(k)} \otimes \boldsymbol{n}^{(k)}, \tag{2.27}$$

$$\boldsymbol{P} = \sum_{k=1}^{3} \frac{\partial W}{\partial \lambda_k} \boldsymbol{n}^{(k)} \otimes \boldsymbol{N}^{(k)}, \tag{2.28}$$

where $\boldsymbol{n}^{(k)}$ are the unit eigenvectors of the left Cauchy–Green deformation tensor ($\boldsymbol{b}$), for which $\boldsymbol{N}^{(k)} = \lambda_a \boldsymbol{F}^{-1} \boldsymbol{n}^{(k)}$ holds. Based on equations (2.25) - (2.28) the principal stresses can be expressed as

$$S_k = \frac{1}{\lambda_k} \frac{\partial W}{\partial \lambda_k}, \quad \sigma_k = \frac{\lambda_k}{J} \frac{\partial W}{\partial \lambda_k}, \quad \tau_k = \lambda_k \frac{\partial W}{\partial \lambda_k}, \quad P_k = \frac{\partial W}{\partial \lambda_k}, \qquad k = 1, 2, 3. \tag{2.29}$$

## 2.2 Ogden–Hill's hyperelastic model

Several hyperelastic models are available in the literature, which are usually based on phenomenological or morphological considerations and developed usually experimentally in order to describe the stress-strain response of a certain type of hyperelastic material properly. It should be noted that there is no commonly accepted hyperelastic model. In order to choose the proper hyperelastic material model for a certain material, the mechanical behaviour and properties of the investigated material should always be taken into consideration.

The development of hyperelastic material models was indicated by the need of modelling rubber-like materials. Rubber-like materials exhibit large deformations, while the volume change is approximately zero. In case of small-strain theory for the Poisson's ratio the approximation $\nu \approx 0{,}5$ can be applied. This simplifies the kinematic description of the deformation, since the number of the unknown parameters decreases. However, the bulk modulus corresponding to the volumetric strain will be infinity, which leads to computational problems in finite element analysis. To solve this problem, instead of the perfectly *incompressible* hyperelastic models, a slightly modified so-called *nearly-incompressible* hyperelastic models are applied, which allow small volumetric deformations, thus the numerical simulations can be performed.

Compared to rubber-like materials, the deformation of polymer foams show large deformations and large volumetric strains as well. Therefore, the hyperelastic material models developed for rubber-like materials cannot be applied for polymer foams. The volumetric strain is so significant, that mainly in case of the so-called open-cell polymer foams the cross-directional strains can be neglected in case of uniaxial compression, therefore for the Poisson's ratio the

$$\nu \approx 0 \tag{2.30}$$

approximation is applied [2], [3]. In this thesis the investigated memory foam material is an open-cell polymer foam, therefore in the further calculations the approximation in (2.30) will be used.

There is a limited number of so-called *compressible* hyperelastic models, which describe the large volumetric deformations accurately. There is only one widely applied compressible hyperelastic model in the literature, which is also implemented the most popular commercial finite element software (Abaqus [5], Ansys [14], Msc Marc [15]), although the name of this material model is not uniform. The model referred as "*Hyperfoam*" in Abaqus, "*Ogden foam*" in Ansys and "*Rubber foam*" in Msc Marc. The material model named in the literature differently as well, because its introduction can be related to three different authors, but mostly the *Ogden–Hill's hyperelastic model* is referred.

### 2.2.1 The history of the Ogden–Hill's hyperelastic model

Ogden investigated the hyperelastic modelling of compressible materials in his paper in 1972 [16]. He provided a hyperelastic material model, in which a former compressible hyperelastic material model for rubber-like materials was extended with an additional unknown function $f(\lambda_1, \lambda_2, \lambda_3)$, which describes the strain energy ($W$) corresponding to the volumetric strain. In his formulation the strain energy function of for compressible materials is written as

$$W = \sum_{i=1}^{N} \frac{\bar{\mu}_i}{\alpha_i} \left(\lambda_1^{\alpha_i} + \lambda_2^{\alpha_i} + \lambda_3^{\alpha_i} - 3\right) + f(\lambda_1, \lambda_2, \lambda_3), \tag{2.31}$$

where $N$ denotes the order of the hyperelastic model, $\alpha_i$ and $\bar{\mu}_i$ material parameters. Later, in 1978 Hill in his contribution [17] expressed the volumetric part in the Ogden model (2.31) as

$$f(\lambda_1, \lambda_2, \lambda_3) = \sum_{i=1}^{N} \frac{\bar{\mu}_i}{\alpha_i} \frac{1-2\nu}{\nu} \left(J^{-\frac{\nu}{1-2\nu}\alpha_i} - 1\right), \tag{2.32}$$

which can be substituted back into (2.31), this yields

$$W = \sum_{i=1}^{N} \frac{\bar{\mu}_i}{\alpha_i} \left(\lambda_1^{\alpha_i} + \lambda_2^{\alpha_i} + \lambda_3^{\alpha_i} - 3 + \frac{1-2\nu}{\nu} \left(J^{-\frac{\nu}{1-2\nu}\alpha_i} - 1\right)\right). \tag{2.33}$$

In this formulation there are three material parameters $\alpha_i$, $\bar{\mu}_i$ and $\nu$, where $\alpha_i$ and $\bar{\mu}_i$ are joint parameters, therefore the model contains $2N + 1$ material parameters. This material model was rewritten by Storakers [18], in his formulation a new parameter was introduced, thus

$$W = \sum_{i=1}^{N} \frac{\bar{\mu}_i}{\alpha_i} \left(\lambda_1^{\alpha_i} + \lambda_2^{\alpha_i} + \lambda_3^{\alpha_i} - 3 + \frac{1}{n} \left(J^{-n\alpha_i} - 1\right)\right), \tag{2.34}$$

where the new parameter $n$ related directly to the Poisson's ratio as

$$n = \frac{\nu}{1-2\nu}. \tag{2.35}$$

The formulation of the material model available in Abaqus [5] is based on the formulation of Storakers in (2.34), but the parameters are defined in a different way. According to Abaqus the strain energy function is defined as

$$W = \sum_{i=1}^{N} \frac{2\mu_i}{\alpha_i^2} \left(\lambda_1^{\alpha_i} + \lambda_2^{\alpha_i} + \lambda_3^{\alpha_i} - 3 + \frac{1}{\beta_i} \left(J^{-\alpha_i\beta_i} - 1\right)\right). \tag{2.36}$$

It should be noted that the $\mu_i$ parameters in the ABAQUS formulation are not equal with the $\bar{\mu}_i$ parameters applied in (2.34). Besides, a significant difference is that ABAQUS defines the $n$ parameter to be joint to $\alpha_i$ and $\mu_i$ parameters, thus $N$ different $n$ parameters are presented in the material model. To emphasize this difference ABAQUS uses $\beta_i$ parameters instead of $n$. Furthermore the $\mu_i$ and $\beta_i$ parameters in this formulation can directly be related to the initial shear ($\mu_0$) and the initial bulk ($K$) moduli as

$$\mu_0 = \sum_{i=1}^{N} \mu_i > 0, \qquad K = \sum_{i=1}^{N} 2\mu_i \left(\frac{1}{3} + \beta_i\right) > 0, \tag{2.37}$$

which also define criteria for the possible values of the material parameters $\mu_i$ and $\beta_i$. The detailed derivation is provided in *Appendix* A. During the further calculations the ABAQUS formulation of the Ogden–Hill's hyperelastic model in (2.36) will be applied.

### 2.2.2 Stress solutions

The stress solutions of the time-independent Ogden–Hill's hyperelastic material model can be obtained by substituting the previously defined strain energy function in (2.36) into (2.29). After expressing the partial derivatives the principal stress solutions become

$$\tau_k = \sum_{i=1}^{N} \frac{2\mu_i}{\alpha_i} \left(\lambda_k^{\alpha_i} - J^{-\alpha_i \beta_i}\right), \tag{2.38}$$

$$\sigma_k = \frac{1}{J} \sum_{i=1}^{N} \frac{2\mu_i}{\alpha_i} \left(\lambda_k^{\alpha_i} - J^{-\alpha_i \beta_i}\right), \tag{2.39}$$

$$S_k = \sum_{i=1}^{N} \frac{1}{\lambda_k^2} \frac{2\mu_i}{\alpha_i} \left(\lambda_k^{\alpha_i} - J^{-\alpha_i \beta_i}\right), \tag{2.40}$$

$$P_k = \sum_{i=1}^{N} \frac{1}{\lambda_k} \frac{2\mu_i}{\alpha_i} \left(\lambda_k^{\alpha_i} - J^{-\alpha_i \beta_i}\right), \tag{2.41}$$

where the load is characterised by the $\lambda_k$ principal stretch inputs. In the coordinate system of the principal stretches the deformation gradient and the Kirchhoff stress tensor will have the form

$$\mathbf{F} = \begin{bmatrix} \lambda_1 & 0 & 0 \\ 0 & \lambda_2 & 0 \\ 0 & 0 & \lambda_3 \end{bmatrix}; \qquad \boldsymbol{\tau} = \begin{bmatrix} \tau_1 & 0 & 0 \\ 0 & \tau_2 & 0 \\ 0 & 0 & \tau_3 \end{bmatrix}, \tag{2.42}$$

thus the volume ratio becomes $J = \det \mathbf{F} = \lambda_1 \lambda_2 \lambda_3$.

## 2.3 Material stability

The material parameters in the Ogden–Hill's compressible hyperelastic material model cannot be chosen freely. Some criteria have already been formulated in (2.37), but in order to receive physically acceptable results the material model should be stable for all strains. Otherwise, the numerical simulation (finite element analysis) will be inaccurate or may not converge. This defines new criteria for the material parameters, which has to be checked after the parameter fitting process. One possible method to check the material stability is the Drucker-stability criteria, which is also implemented in ABAQUS [5].

The Drucker-stability criteria states, that the strain energy has to increase for any increment in the strain. Based on the ABAQUS formulation [5], the criteria can be expressed as

$$\mathrm{d}\boldsymbol{\tau} : \mathrm{d}\mathbf{h} > 0, \tag{2.43}$$

where $\mathbf{h} = \ln \mathbf{V}$ is the spatial logarithmic strain tensor [5]. In case of isotropic material the relation can be expressed in the coordinate system of the principal stretches as

$$\sum_{k=1}^{3} \mathrm{d}\tau_k \mathrm{d}h_k = \mathrm{d}\tau_1 \mathrm{d}h_1 + \mathrm{d}\tau_2 \mathrm{d}h_2 + \mathrm{d}\tau_3 \mathrm{d}h_3 > 0, \tag{2.44}$$

where $\mathrm{d}h_k$ are the logarithmic strain increments and $\mathrm{d}\tau_k$ the corresponding principal Kirchhoff stress increments. The corresponding strain and stress increments are related to each other via the constitutive equation of the material model. Therefore, let us introduce the following matrix notation

$$\mathrm{d}\boldsymbol{\tau}_{\mathbf{k}} = \begin{bmatrix} \mathrm{d}\tau_1 \\ \mathrm{d}\tau_2 \\ \mathrm{d}\tau_3 \end{bmatrix}; \qquad \mathrm{d}\mathbf{h}_{\mathbf{k}} = \begin{bmatrix} \mathrm{d}h_1 \\ \mathrm{d}h_2 \\ \mathrm{d}h_3 \end{bmatrix}. \tag{2.45}$$

Using the notation above, the stress and the stain increment vectors can be related as

$$\mathrm{d}\boldsymbol{\tau}_{\mathbf{k}} = \mathbf{D}\mathrm{d}\mathbf{h}_{\mathbf{k}}, \tag{2.46}$$

where the $\mathbf{D}$ matrix is defined from principal stresses (2.38)-(2.41) as

$$\mathbf{D} = \begin{bmatrix} D_{11} & D_{12} & D_{13} \\ D_{21} & D_{22} & D_{23} \\ D_{31} & D_{32} & D_{33} \end{bmatrix} = \sum_{i=1}^{N} 2\mu_i \begin{bmatrix} \lambda_1^{\alpha_i} + A_i & A_i & A_i \\ A_i & \lambda_2^{\alpha_i} + A_i & A_i \\ A_i & A_i & \lambda_3^{\alpha_i} + A_i \end{bmatrix}, \tag{2.47}$$

where $A_i = \beta_i J^{-\alpha_i \beta_i}$ [5]. After substituting back (2.46) into the stability criterion (2.43), it gives

$$\mathrm{d}\mathbf{h}_{\mathbf{k}} \mathbf{D} \mathrm{d}\mathbf{h}_{\mathbf{k}} > 0. \tag{2.48}$$

The criterion is satisfied, when $\mathbf{D}$ is positive definite, thus its scalar invariants should be positive. Therefore the criteria for $\mathbf{D}$ become

$$\begin{aligned} I_{\mathbf{D}} &= \mathrm{tr}\mathbf{D} = D_{11} + D_{22} + D_{33} > 0, & (2.49) \\ II_{\mathbf{D}} &= \frac{1}{2}((\mathrm{tr}\mathbf{D})^2 - \mathrm{tr}\mathbf{D}^2) = D_{11}D_{22} + D_{11}D_{33} + D_{22}D_{33} > 0, & (2.50) \\ III_{\mathbf{D}} &= \det \mathbf{D} = D_{11}D_{22}D_{33} > 0. & (2.51) \end{aligned}$$

It should be noted that $\mathbf{D}$ contains the principal stretches ($\lambda_k$), therefore the stability depends on the load as well.

In order to assume, that the fitted material model is stable, the Drucker-stability should be checked for all homogeneous deformations. Alternatively, there is a built-in stability-checking algorithm in ABAQUS, which reports the material stability for all homogeneous deformations into the `Job.dat` file. During our calculation this latter method will be applied [5].

# 3
# Viscoelastic material modelling

The time-dependent behaviour of polymer foams can be described using special viscoelastic material models. These models are based on the description of the most significant viscoelastic phenomena: the relaxation or the creep. The material models consist of two parts: a hyperelastic and a viscoelastic part [5], where the time-dependent behaviour is characterised by the viscoelastic model, while the time-independent hyperelastic behaviour is modelled using the previously introduced Ogden–Hill's hyperelastic model. Since, the time dependent (or rate dependent) deformations are characterised by large strains and large deformations, the small-strain linear viscoelastic material models cannot be applied. In case of finite strains the so-called visco-hyperelastic modelling approach has to be followed.

To understand the finite strain visco-hyperelastic constitutive equation for compressible materials, firstly the viscoelastic material behaviour and the linear viscoelastic model should be analysed, which is valid only for small strains, and then we can reformulate it using finite strain formalism.

## 3.1 Viscoelastic material behaviour

Elastic materials are capable to store the potential energy during the loading process and when the load is removed, the original shape is retrieved immediately. Compared to this, the viscoelastic materials have viscous properties as well, which means that some energy is dissipated in the material during the loading. Therefore, the mechanical behaviour of such materials became time-dependent, thus the original shape is retrieved only in "infinite" time after the unloading. In case of cyclic loading hysteresis can be observed in the stress-strain characteristic ($\sigma - \varepsilon$), namely the uploading and the downloading processes follow different path on the stress-strain characteristic. Time-dependency also means that the strain rate ($\dot{\varepsilon}$) influences the overall material behaviour, since the bigger the strain rate the higher the resulting stress. The above mentioned phenomena are illustrated in Fig. (3.1) [3].

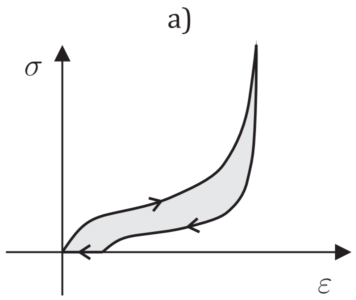


**Figure 3.1:** Properties of viscoelastic material behaviour: a) hysteresis during cyclic load and b) the effect of increasing strain rate

The two most significant phenomena of the viscoelastic material behaviour are the stress relaxation and the creep. In case of stress relaxation the stress decays exponential-likely, when the strain is kept constant ($\varepsilon_0$), while in case of creep the stress is kept constant ($\sigma_0$), which cause increasing strains in an exponential-like way (see Fig. 3.2) [2]. Both phenomena can be characterised by a $\tau$ time constant, which is referred as relaxation or retardation time, respectively. These phenomena are especially significant from the material modelling point of view, because the material models, that describe the time-dependent behaviour, are based on the modelling of the stress relaxation or the creep. In my thesis viscoelastic models with stress relaxation-based formulations will be used [8].

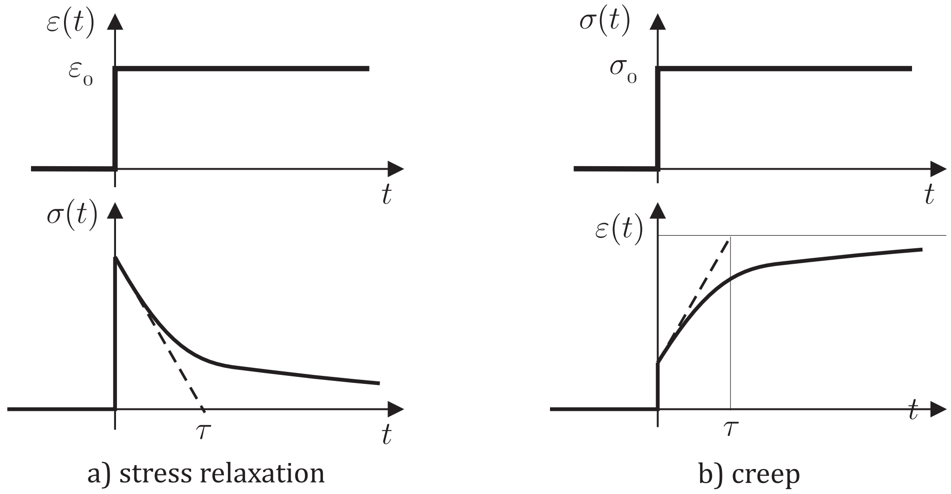


**Figure 3.2:** The phenomena of stress relaxation and creep

### 3.1.1 The mechanical model of relaxation in 1D

The behaviour of one-dimensional linear viscoelastic materials can be modelled with a system of springs and dampers. The state variables of the systems are the $\sigma(t)$ stress and the $\varepsilon(t)$ strain. The ideal spring (the Hooke-element) relates the state variables as

$$\sigma(t) = E\varepsilon(t), \tag{3.1}$$

where $E$ is the elastic modulus. The linear damping (*dashpot)* defines connection between the strain rate $\dot{\varepsilon}(t)$ and the stress $\sigma(t)$ as

$$\dot{\varepsilon}(t) = \frac{\sigma(t)}{\eta}, \tag{3.2}$$

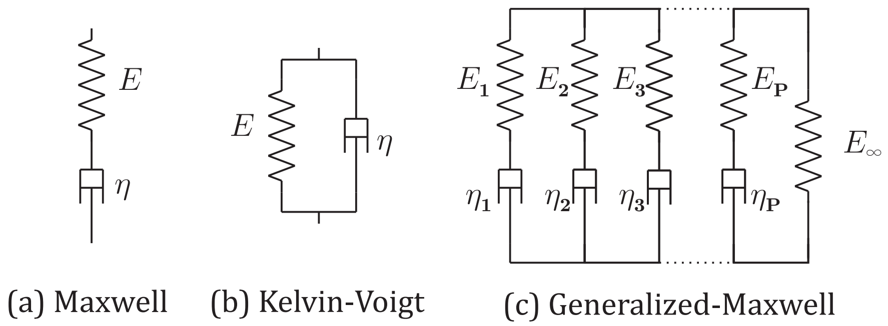


**Figure 3.3:** Mechanical models of time-dependent material behaviour

where $\eta$ is the viscosity [19]. The serial configuration of the spring and the linear damping gives the so-called MAXWELL-element (see Fig. 3.3/a) [19], where the governing differential equation of the state variables becomes

$$\dot{\varepsilon}(t) = \frac{\sigma(t)}{\eta} + \frac{\dot{\sigma}(t)}{E}. \tag{3.3}$$

On the other hand, the parallel configuration of the spring and the dashpot is called KELVIN-VOIGT-element (see Fig. 3.3/b) [19], while the corresponding differential equation can be obtained as

$$\sigma(t) = E\varepsilon(t) + \eta\dot{\varepsilon}(t). \tag{3.4}$$

The viscoelastic material behaviour can be characterised with the differential equations in (3.3) and (3.4), which are the constitutive equations of linear viscoelasticity. For more complex cases, the so-called *Generalized-Maxwell* model is applied, in which several ($P$) MAXWELL-elements and one HOOKE-element are assembled in parallel (see Fig. 3.3/c). In this approach the HOOKE-element models the long-term elastic behaviour (i.e. when the load in infinitely slow), where $E_\infty$ is the long-term elastic modulus [2].

### 3.1.2 The stress solution for 1D loading

In the Generalized-Maxwell model the number of parallel MAXWELL-elements is $P$, while $\eta_k$ and $E_k$ denotes the parameters in the MAXWELL-elements, respecitively. Using these parameters we can introduce a time parameter for each element, namely $\tau_k = \eta_k/E_k$. This leads, that the resultant time-dependent elastic modulus $E(t)$ can be expressed as

$$E(t) = E_\infty + \sum_{k=1}^{P} E_k \exp\left[\frac{-t}{\tau_k}\right], \tag{3.5}$$

which is written using the so-called Prony-series representation [19]. The stress solution can be obtained as the solution of the viscoelastic model, for a prescribed $\varepsilon(t)$ strain history. The model defines the stress solution in 1D as a convolution (or hereditary) integral of the strain rate $\dot{\varepsilon}(t)$ and the time-dependent elastic modulus in (3.5), thus

$$\sigma(t) = \int_0^t E(t-s)\dot{\varepsilon}(s)\mathrm{d}s. \tag{3.6}$$

The formula can be rewritten in an alternative, but equivalent form, which is based on the instantaneous elastic response instead. In this form the instantaneous elastic and the viscoelastic contributions can be separated, therefore using the formalism in Abaqus [5] the convolution integral is defined as

$$\sigma(t) = \sigma_0(t) - \sum_{k=1}^{P} \frac{e_k}{\tau_k} \int_0^t \sigma_0(t-s) \exp\left[\frac{-s}{\tau_k}\right] \mathrm{d}s, \tag{3.7}$$

where the instantaneous stress response $\sigma_0(t)$ can be obtained from the strain input and the instantaneous elastic modulus $E_0$ as,

$$\sigma_0(t) = E_0 \varepsilon(t). \tag{3.8}$$

The above introduced model also contains the so-called relative elastic moduli $e_k$, which are defined as

$$e_k = \frac{E_k}{E_0}. \tag{3.9}$$

## 3.2 Finite strain viscoelasticity

The mechanical characteristic of the investigated open-cell polymer foams require obtaining viscoelastic material models using finite strain theory. As a consequence the linear viscoelastic constitutive equation in (3.7) cannot be applied for polymer-foams. Instead, the so-called visco-hyperelastic modelling approach has to be followed. These material models combines the hyperelastic material model for nonlinear materials with finite strains and the time-dependent viscoelastic material model [5].

The visco-hyperelastic material model can be obtained by reformulating the linear viscoelastic material model using finite strain theory. A possible formulation of such visco-hyperelastic materials are provided by Abaqus [5]. It should be noted, that in Abaqus version 6.9, the material model was updated and reformulated, but for the *Hyperfoam* (Ogden–Hill's) hyperelastic material model the implementation is remained the previous (as in Abaqus version 6.8) [9]. Therefore, in my calculations the original formulation is applied. According to the Abaqus formalism, the constitutive equation is defined for the Kirchhoff stress tensor ($\boldsymbol{\tau}$) [5], where for compressible materials the instantaneous Kirchhoff stress tensor ($\boldsymbol{\tau}_0$) can be splitted into hydrostatic and deviatoric parts as

$$\boldsymbol{\tau}_0(t) = \boldsymbol{\tau}_0^D(\bar{\mathbf{F}}(t)) + \boldsymbol{\tau}_0^H(J(t)), \tag{3.10}$$

where the hydrostatic part is the function of the $J$ volume ratio, while the deviatoric part is related to the so-called distortional deformation gradient ($\bar{\mathbf{F}}$). The distortional deformation gradient can be directly obtained from the deformation gradient $\mathbf{F}$, as

$$\bar{\mathbf{F}} = \mathbf{F} J^{-1/3}. \tag{3.11}$$

In Abaqus version 6.7 [5] the visco-hyperelastic constitutive equation corresponding to finite strain materials can be obtained by the following convolution integrals:

$$\boldsymbol{\tau}^D(t) = \boldsymbol{\tau}_0^D(t) + \mathrm{SYMM} \int_0^t \frac{\dot{G}(s)}{G_0} \mathbf{F}_t^{-1}(t-s) \boldsymbol{\tau}_0^D(t-s) \mathbf{F}_t(t-s) \mathrm{d}s, \tag{3.12}$$

$$\boldsymbol{\tau}^H(t) = \boldsymbol{\tau}_0^H(t) + \int_0^t \frac{\dot{K}(s)}{K_0} \boldsymbol{\tau}_0^H(t-s) \mathrm{d}s. \tag{3.13}$$

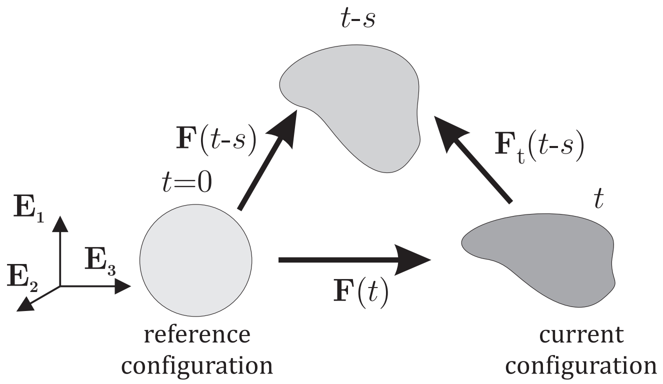


**Figure 3.4:** The representation of the $\mathbf{F}_t(t-s)$ relative deformation gradient

The hereditary integral of the deviatoric part is performed via the *pull-back* $\mathbf{F}_t(t-s)$ and *push-forward* $\mathbf{F}_t^{-1}(t-s)$ operators. In order to ensure objectivity, the system is transformed firstly back into the state corresponding to time $t-s$, where the convolution integral can be performed and then transformed back into the spatial configuration. Finally, the symmetric part of the solution is obtained by using the SYMM operator. The *pull-back* operator, illustrated in Fig. 3.4, is practically a relative deformation gradient defined between the time instants $t-s$ and $t$, therefore

$$\mathbf{F}_t(t-s) = \mathbf{F}(t-s)\mathbf{F}^{-1}(t). \tag{3.14}$$

In the deviatoric part of the governing constitutive equation (3.12) $G(t)$ and $G_0$ are the time-dependent and the instantaneous shear moduli, respectively. Similarly, in the hydrostatic part (3.13) $K(t)$ and $K_0$ defines the time-dependent and the instantaneous bulk moduli, respectively. Similarly to equation (3.5) the time-dependent mechanical moduli can be written using the Prony-series representation as

$$G(t) = G_0\left(g_\infty + \sum_{k=1}^{PG} g_k \exp\left[\frac{-t}{\tau_k^G}\right]\right), \qquad K(t) = K_0\left(k_\infty + \sum_{k=1}^{PK} k_k \exp\left[\frac{-t}{\tau_k^K}\right]\right), \tag{3.15}$$

where $g_k$ and $k_k$ are the relative, while $g_\infty$ and $k_\infty$ are the long-term moduli, respectively. For the so-called relaxation moduli the following condition holds:

$$g_\infty + \sum_{k=1}^{PG} g_k = k_\infty + \sum_{k=1}^{PK} k_k = 1. \tag{3.16}$$

The substitution of (3.15) into the convolution integrals in (3.12) and (3.13) defines the constitutive equation of the material model as

$$\boldsymbol{\tau}^D(t) = \boldsymbol{\tau}_0^D(t) - \mathrm{SYMM}\left[\sum_{k=1}^{PG} \frac{g_k}{\tau_k^G}\int_0^t \mathbf{F}_t^{-1}(t-s)\boldsymbol{\tau}_0^D(t-s)\mathbf{F}_t(t-s)\exp\left[\frac{-s}{\tau_k^G}\right]\mathrm{d}s\right], \tag{3.17}$$

$$\boldsymbol{\tau}^H(t) = \boldsymbol{\tau}_0^H(t) - \sum_{k=1}^{PK}\frac{k_k}{\tau_k^K}\int_0^t \boldsymbol{\tau}_0^H(t-s)\exp\left[\frac{-s}{\tau_k^K}\right]\mathrm{d}s. \tag{3.18}$$

Based on the literature suggestions [5], we assume that the number of parameters in the deviatoric and the hydrostatic parts are equal, thus $PG = PK = P$. Based on the assumption that the shear and the bulk moduli relax equally, it can be considered that the corresponding relative shear and bulk moduli are the same, therefore $g_k = k_k$, furthermore the relaxation parameters are also obtained to be equal, thus $\tau_k^G = \tau_k^K = \tau_k$. After substituting the above introduced conditions into the constitutive equations in (3.17) and (3.18), the final form of the visco-hyperelastic material model for open-cell polymer foams became

$$\boldsymbol{\tau}^D(t) = \boldsymbol{\tau}_0^D(t) - \mathrm{SYMM}\left[\sum_{k=1}^{P} \frac{g_k}{\tau_k} \int_0^t \mathbf{F}_t^{-1}(t-s)\boldsymbol{\tau}_0^D(t-s)\mathbf{F}_t(t-s)\exp\left[\frac{-s}{\tau_k}\right] \mathrm{d}s\right], \tag{3.19}$$

$$\boldsymbol{\tau}^H(t) = \boldsymbol{\tau}_0^H(t) - \sum_{k=1}^{P} \frac{g_k}{\tau_k} \int_0^t \boldsymbol{\tau}_0^D(t-s)\exp\left[\frac{-s}{\tau_k}\right] \mathrm{d}s, \tag{3.20}$$

where the instantaneous stress responses, $\boldsymbol{\tau}_0^D(t)$ and $\boldsymbol{\tau}_0^H(t)$ are adopted from the Ogden–Hill's *Hyperfoam* material model, which was defined in (2.36).

## 3.3 Numerical implementation

The stress solution for visco-hyperelastic materials can be obtained as the solution of the derived constitutive equation in (3.19) and (3.20), where the prescribed $\lambda(t)$ stretch-history in the instantaneous stress response characterize the loading path. During the finite element analysis, it is required to solve the integrals efficiently. Therefore, a numerical integration scheme is also provided by Abaqus [5], where solution is integrated forward in time.

Firstly, let us introduce $\boldsymbol{\tau}_k^D(t)$ and $\boldsymbol{\tau}_k^H(t)$ internal deviatoric and hydrostatic stresses, respectively, which are defined as

$$\begin{aligned}
\boldsymbol{\tau}_k^D(t) &= \mathrm{SYMM}\left[\frac{g_k}{\tau_k} \int_0^t \mathbf{F}_t^{-1}(t-s)\boldsymbol{\tau}_0^D(t-s)\mathbf{F}_t(t-s)\exp\left[\frac{-s}{\tau_k}\right] \mathrm{d}s\right], && (3.21)\\
\boldsymbol{\tau}_k^H(t) &= \frac{g_k}{\tau_k} \int_0^t \boldsymbol{\tau}_0^H(t-s)\exp\left[\frac{-s}{\tau_k}\right] \mathrm{d}s. && (3.22)
\end{aligned}$$

For the deviatoric stresses, the *pull-back*, the *push-forward* and the SYMM operators should also be considered, thus a modified deviatoric stresses should be obtained as

$$\begin{aligned}
\hat{\boldsymbol{\tau}}_0^D(t) &= \mathrm{SYMM}\left[\Delta\mathbf{F}\boldsymbol{\tau}_0^D(t)\Delta\mathbf{F}^{-1}\right], && (3.23)\\
\hat{\boldsymbol{\tau}}_k^D(t) &= \mathrm{SYMM}\left[\Delta\mathbf{F}\boldsymbol{\tau}_k^D(t)\Delta\mathbf{F}^{-1}\right], && (3.24)
\end{aligned}$$

where $\Delta\mathbf{F} = \mathbf{F}_t(t+\Delta t)$. According to the integration scheme applied in Abaqus [5], the stress solution at time $t+\Delta t$ can be calculated as

$$\begin{aligned}
\boldsymbol{\tau}(t+\Delta t) = {} & \left(1 - \sum_{k=1}^{P} a_i g_k\right)\boldsymbol{\tau}_0^D(t+\Delta t) + \sum_{k=1}^{P} b_i g_k \hat{\boldsymbol{\tau}}_0^D(t) + \sum_{k=1}^{P} c_i \hat{\boldsymbol{\tau}}_k^D(t) + \\
& \left(1 - \sum_{k=1}^{P} a_i g_k\right)\boldsymbol{\tau}_0^H(t+\Delta t) + \sum_{k=1}^{P} b_i g_k \boldsymbol{\tau}_0^H(t) + \sum_{k=1}^{P} c_i \boldsymbol{\tau}_k^H(t), && (3.25)
\end{aligned}$$

with

$$a_i = 1 - \frac{\tau_k}{\Delta t}(1-c_i); \quad b_i = \frac{\tau_k}{\Delta t}(1-c_i) - c_i; \quad c_i = \exp\left[\frac{-\Delta t}{\tau_k}\right]. \tag{3.26}$$

Therefore the stress solution at time $t+\Delta t$ can be derived from the intantaneous and internal stress values at time instant $t$ and $t+\Delta t$. The detailed derivation of the integration scheme is provided in *Appendix* B.

# 4

# Closed-form stress solutions

As it was introduced in *Chapter* 3, the mechanical behaviour of polymer foams can be modelled using visco-hyperelatic material models, where the corresponding hyperelastic constitutive equation is the Ogden–Hill's *Hyperfoam* model. Nevertheless, the model is obtained using the hereditary integral of the input stetch-history function, therefore to obtain analytically the stress solution, the convolution integrals in (3.19) and (3.20) should be solved.

In the literature, the closed-form solution corresponding any particular loading case has not been provided yet, since the solution of the integral is quite complex. The main goal of this thesis is to provide the closed-form solutions for the most common homogeneous deformations: uniaxial, equibiaxial and volumetric compressions [9],[10].

## 4.1 Homogeneous deformations

Firstly, let us summarize the basic homogeneous deformations, for which the closed form solutions are to be provided. In these cases the deformation is characterised by the deformation gradient $\boldsymbol{F}$. Based on the deformation gradient the principal stretches can also be obtained ($\lambda_k$), which in case of time-dependent material behavior are considered to be time functions, thus

$$\lambda_k = \lambda_k(t). \tag{4.1}$$

Based on the principal stretches, the instantaneous (time-independent) Kirchhoff stress tensor ($\boldsymbol{\tau}_0(t)$), which appears in the visco-hyperelatic constitutive equation, can be expressed based on the Ogden–Hill's hyperelastic material model in (2.38). During our calculation the assumtion $\beta_i = 0$ will be applied as it was introduced for open-cell polymer foams in (2.30). Therefore, the principal Kirchhoff stresses obtained from (2.38) can be simplified as

$$\tau_k = \sum_{i=1}^{N} \frac{2\mu_i}{\alpha_i} \left(\lambda_k^{\alpha_i} - 1\right). \tag{4.2}$$

### 4.1.1 Uniaxial compression

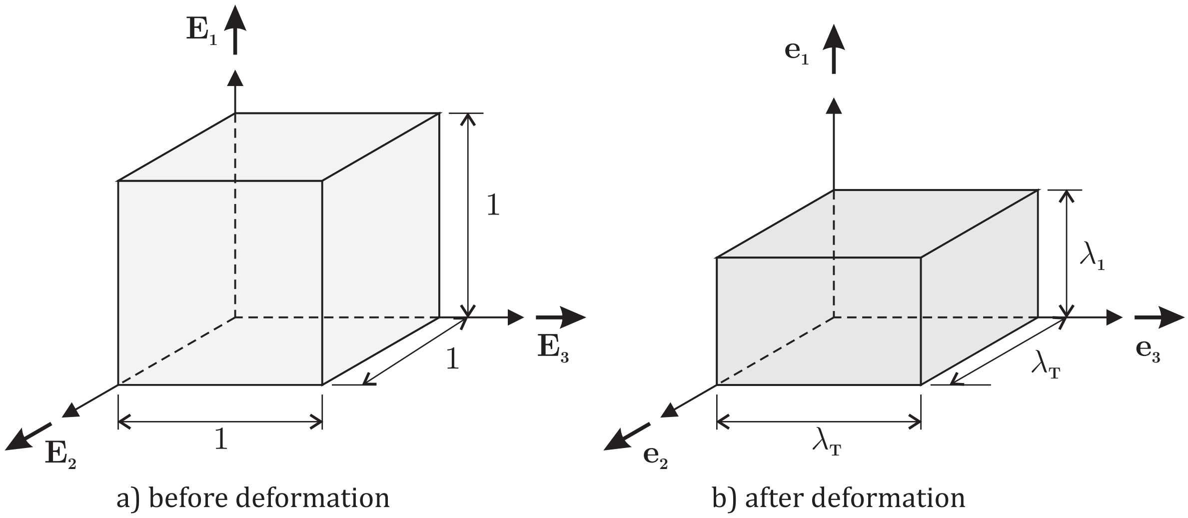


**Figure 4.1:** The kinematics of uniaxial compression

In case of uniaxial compression, the body is compressed in only one direction. This direction is called as longitudinal direction, and the corresponding stretch is denoted as $\lambda_1$. In the other two principal directions, which are referred as transversal directions, no load is applied. For isotropic materials the transversal stretches are identical, thus $\lambda_2 = \lambda_3 = \lambda_T$. Additionally, the body can deform freely in these directions, which leads that the transversal stresses are zero. The kinematics of the loading case is presented in Fig. 4.1. Therefore, the deformation gradient becomes

$$\mathbf{F} = \begin{bmatrix} \lambda_1 & 0 & 0 \\ 0 & \lambda_T & 0 \\ 0 & 0 & \lambda_T \end{bmatrix} = \begin{bmatrix} \lambda_1 & 0 & 0 \\ 0 & 1 & 0 \\ 0 & 0 & 1 \end{bmatrix}, \tag{4.3}$$

where $\lambda_T \equiv 1$, because the $\beta_i = 0$ assumtion is applied. Based on the description of uniaxial comrpession the Kirchhoff stress tensor can be written as

$$\boldsymbol{\tau} = \begin{bmatrix} \tau_1 & 0 & 0 \\ 0 & 0 & 0 \\ 0 & 0 & 0 \end{bmatrix}. \tag{4.4}$$

By substituting, the principal stretches back into the Ogden–Hill's constitutive equation in (4.2), the instantaneous principal Kirchhoff stress solution can be expressed as

$$\boldsymbol{\tau}_0(t) = \begin{bmatrix} \tau_0(t) & 0 & 0 \\ 0 & 0 & 0 \\ 0 & 0 & 0 \end{bmatrix} = \begin{bmatrix} \sum_{i=1}^{N} \frac{2\mu_i}{\alpha_i} \left(\lambda^{\alpha_i}(t) - 1\right) & 0 & 0 \\ 0 & 0 & 0 \\ 0 & 0 & 0 \end{bmatrix}. \tag{4.5}$$

It should be noted, that for $\beta_i = 0$ case the uniaxial compression is identical with the so-called confined uniaxial deformation case, in which the stretches kept constant in the transversal direction. In this case the body cannot deform freely in the transversal directions, thus stress appears. However, when the Poisson's ratio is neglected, the load has no effect in the transversal directions, this leads that the confined compression has the same kinematic description as the orginal uniaxial compression.

### 4.1.2 Equibiaxial compression

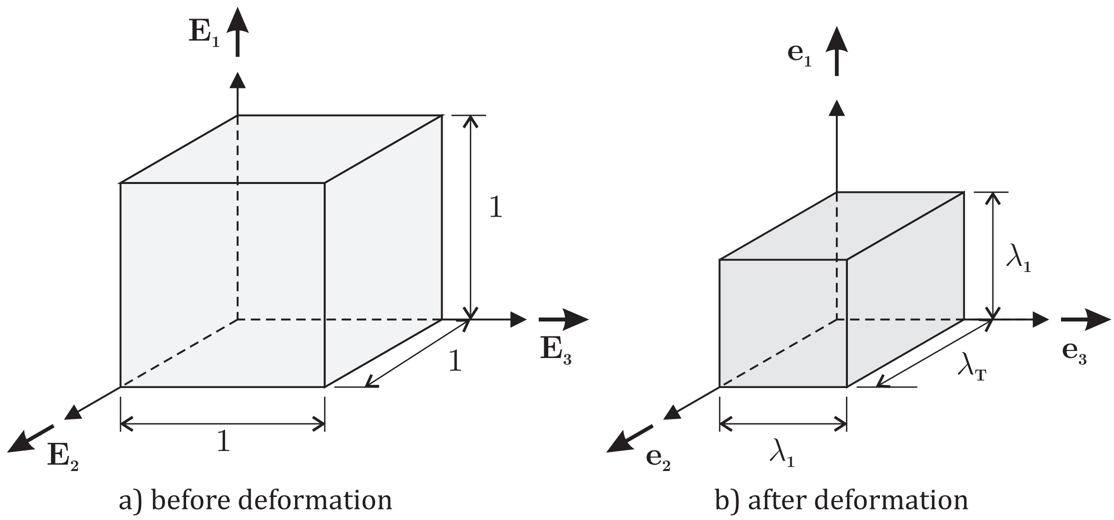


**Figure 4.2:** The kinematics of equibiaxial compression

In this loading case the body is compressed simultaneously in two directions, in which the corresponding principal stretches are denoted as $\lambda_1 = \lambda_2$. In the third (transversal) direction no external load is added, thus the body can deform freely. Fig. 4.2 presents the kinematics of the equibiaxial case. Then, the deformation gradient can be written as

$$\mathbf{F} = \begin{bmatrix} \lambda_1 & 0 & 0 \\ 0 & \lambda_2 & 0 \\ 0 & 0 & \lambda_T \end{bmatrix} = \begin{bmatrix} \lambda_1 & 0 & 0 \\ 0 & \lambda_1 & 0 \\ 0 & 0 & 1 \end{bmatrix}, \tag{4.6}$$

where $\lambda_T \equiv 1$, while the Kirchhoff stress tensor can be obtained as

$$\boldsymbol{\tau} = \begin{bmatrix} \tau_1 & 0 & 0 \\ 0 & \tau_2 & 0 \\ 0 & 0 & 0 \end{bmatrix} = \begin{bmatrix} \tau_1 & 0 & 0 \\ 0 & \tau_1 & 0 \\ 0 & 0 & 0 \end{bmatrix}. \tag{4.7}$$

Applying the relations of the *Hyperfoam* model in (4.2), the instantaneous principal Kirchhoff stress solution becomes

$$\boldsymbol{\tau}_0\,(t) = \begin{bmatrix} \tau_0\,(t) & 0 & 0 \\ 0 & \tau_0\,(t) & 0 \\ 0 & 0 & 0 \end{bmatrix} = \begin{bmatrix} \sum\limits_{i=1}^{N} \dfrac{2\mu_i}{\alpha_i} \left(\lambda^{\alpha_i}\,(t) - 1\right) & 0 & 0 \\ 0 & \sum\limits_{i=1}^{N} \dfrac{2\mu_i}{\alpha_i} \left(\lambda^{\alpha_i}\,(t) - 1\right) & 0 \\ 0 & 0 & 0 \end{bmatrix}. \tag{4.8}$$

It can be observed that in the periously derived instantaneous Kirchhoff stress tensor the corresponding $\tau_0\,(t)$ stress solutions ($\boldsymbol{\tau}_0\,(t)_{11}$ and $\boldsymbol{\tau}_0\,(t)_{22}$) are not only identical with each other, but with the stress solution derived in equation (4.5) for uniaxial compression. Therefore, in the further calculations the equibiaxial case can be directly related to the uniaxial case.

### 4.1.3 Volumetric compression

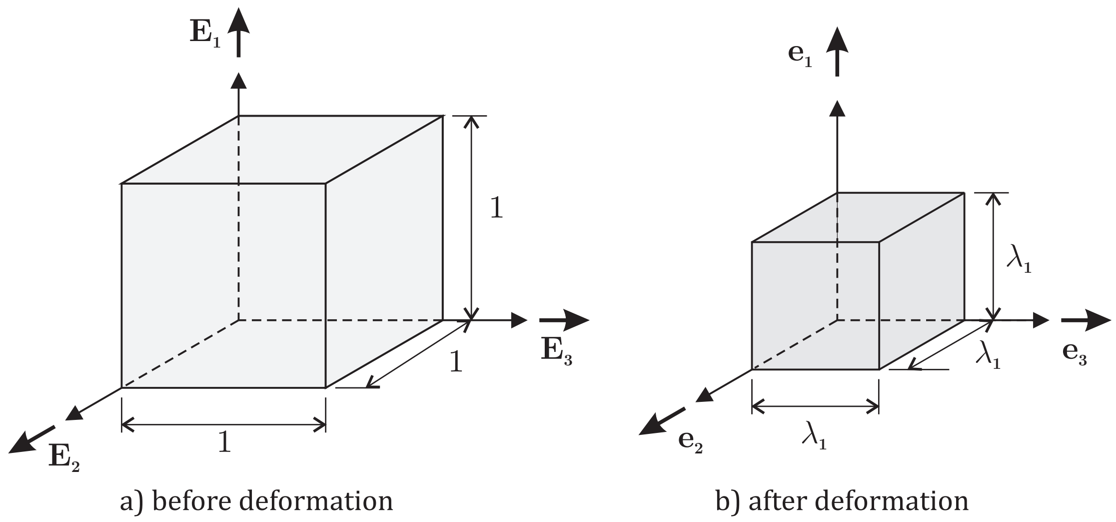


**Figure 4.3:** The kinematics of volumetric compression

In this loading case the body is compressed from each directions in the same way, therefore the principal stretches can be related as $\lambda_1 = \lambda_2 = \lambda_3$ (see Fig. 4.3). Thus, the deformation gradient becomes

$$\mathbf{F} = \begin{bmatrix} \lambda_1 & 0 & 0 \\ 0 & \lambda_2 & 0 \\ 0 & 0 & \lambda_3 \end{bmatrix} = \begin{bmatrix} \lambda_1 & 0 & 0 \\ 0 & \lambda_1 & 0 \\ 0 & 0 & \lambda_1 \end{bmatrix}. \tag{4.9}$$

Due to the isotropy, the stresses will be identical as well, thus the Kirchhoff stress tensor can be expressed as

$$\boldsymbol{\tau} = \begin{bmatrix} \tau_1 & 0 & 0 \\ 0 & \tau_2 & 0 \\ 0 & 0 & \tau_3 \end{bmatrix} = \begin{bmatrix} \tau_1 & 0 & 0 \\ 0 & \tau_1 & 0 \\ 0 & 0 & \tau_1 \end{bmatrix}. \tag{4.10}$$

Substituting back the relations of the hyperelastic material model in (4.2), the instantaneous principal Kirchhoff stress solution becomes

$$\begin{aligned} \boldsymbol{\tau}_0 (t) &= \begin{bmatrix} \tau_0 (t) & 0 & 0 \\ 0 & \tau_0 (t) & 0 \\ 0 & 0 & \tau_0 (t) \end{bmatrix} = \\ & \begin{bmatrix} \sum_{i=1}^{N} \frac{2\mu_i}{\alpha_i} \left(\lambda^{\alpha_i} (t) - 1\right) & 0 & 0 \\ 0 & \sum_{i=1}^{N} \frac{2\mu_i}{\alpha_i} \left(\lambda^{\alpha_i} (t) - 1\right) & 0 \\ 0 & 0 & \sum_{i=1}^{N} \frac{2\mu_i}{\alpha_i} \left(\lambda^{\alpha_i} (t) - 1\right) \end{bmatrix}. \end{aligned} \tag{4.11}$$

The result also suggests the same as in case of equibiaxial compression. The elements in the diagonal are identical with each other and furthermore with the stress solution in equation (4.5). Consequently, the stress solution of the volumetric case can also be related to the solution of uniaxial compression.

### 4.1.4 Simple shear

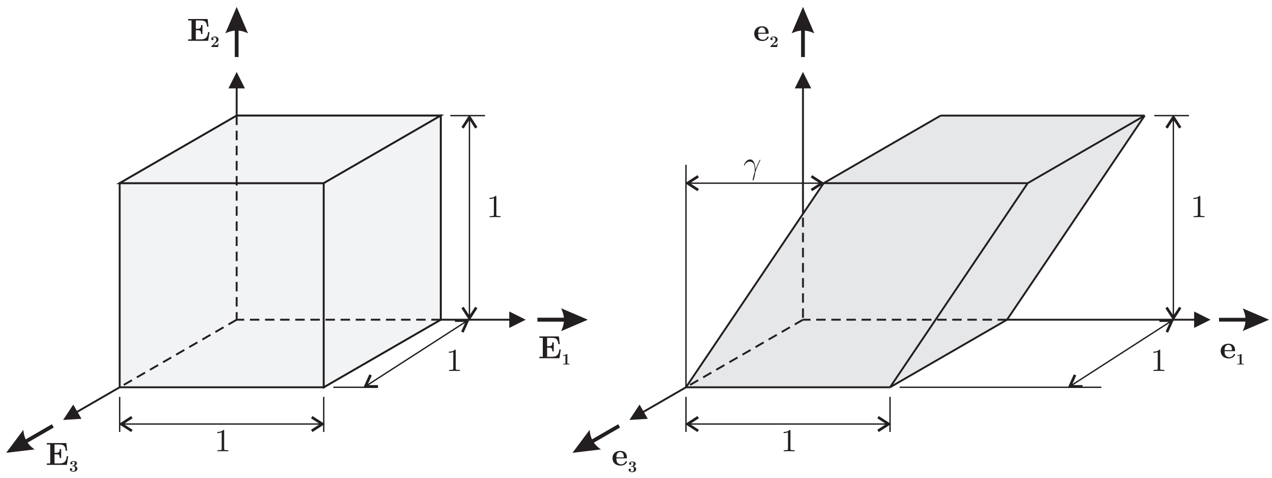


**Figure 4.4:** The kinematics of volumetric compression

In case of simple shear, the upper side of the body is translated with $\gamma$, while the deformations in all other directions are confined. The kinematics of the deformation is presented in Fig. 4.4. Therefore, in the original coordinate system, the deformation gradient become

$$\mathbf{F}_0 = \begin{bmatrix} 1 & \gamma & 0 \\ 0 & 1 & 0 \\ 0 & 0 & 1 \end{bmatrix}, \tag{4.12}$$

which also means that the volume ratio $J = 1$, i.e. the volume does not change. In the coordinate system of the principal stretches the deformation gradient $\mathbf{F}$ can be expressed as

$$\mathbf{F} = \begin{bmatrix} \lambda_1 & 0 & 0 \\ 0 & \lambda_2 & 0 \\ 0 & 0 & \lambda_T \end{bmatrix} = \begin{bmatrix} \lambda_1 & 0 & 0 \\ 0 & \lambda_2 & 0 \\ 0 & 0 & 1 \end{bmatrix}, \tag{4.13}$$

which means, the Kirchhoff stress tensor $\boldsymbol{\tau}$ can be written as

$$\boldsymbol{\tau} = \begin{bmatrix} \tau_1 & 0 & 0 \\ 0 & \tau_2 & 0 \\ 0 & 0 & 0 \end{bmatrix}. \tag{4.14}$$

In order to obtain $\tau_1$ and $\tau_2$ stresses, the principal direction should be determined. Using eigenvalue and eigenvector calculations the principal stretches become

$$\lambda_1 = \frac{1}{2}\left(\gamma + \sqrt{\gamma^2 + 4}\right), \tag{4.15}$$

$$\lambda_2 = \frac{1}{2}\left(-\gamma + \sqrt{\gamma^2 + 4}\right), \tag{4.16}$$

$$\lambda_3 = 1. \tag{4.17}$$

In this case the $\gamma(t)$ function characterise the time-history of the deformation. Substitution of equations in (4.15)-(4.17) into the hyperelastic constitutive equation in (4.2) gives for the instantaneous Kirchhoff stress tensor

$$\boldsymbol{\tau}_0(t) = \begin{bmatrix} \tau_1(t) & 0 & 0 \\ 0 & \tau_2(t) & 0 \\ 0 & 0 & 0 \end{bmatrix} = \begin{bmatrix} \sum_{i=1}^{N} \frac{2\mu_i}{\alpha_i}\left(\lambda_1^{\alpha_i}(t)-1\right) & 0 & 0 \\ 0 & \sum_{i=1}^{N} \frac{2\mu_i}{\alpha_i}\left(\lambda_2^{\alpha_i}(t)-1\right) & 0 \\ 0 & 0 & 0 \end{bmatrix}, \tag{4.18}$$

where $\lambda_1(t) = \frac{1}{2}\left(\gamma(t) + \sqrt{\gamma^2(t)+4}\right)$ and $\lambda_2(t) = \frac{1}{2}\left(-\gamma(t) + \sqrt{\gamma^2(t)+4}\right)$. Unfortunately, these result could not be related to solution of the uniaxial compression case in (4.5), furthermore it can be clearly seen that the corresponding instantaneous stress responses are significantly more complex than previous ones. Consequently, the stress response could not be solved analytically for the simple shear case.

## 4.2 Solution of the hereditary integral

Based on the previously derived expressions, the closed-form stress response of the visco-hyperelastic material can be obtained as the analytical solution of the hereditary integrals in (3.19) and (3.20). The analytical solvability of the convolution integrals strongly depend on the loading case, since the solution can be derived in closed-form only for the simplest deformations and strain histories. In the literature some attempts can be found, where the closed-form solution is derived for much simpler visco-hyperelastic model for rubber-like materials [8], but no analytical solution has been provided yet for the visco-hyperelastic material model using the *Hyperfoam* hyperelastic model . However, in case of open-cell polymer foams (where $\beta_i = 0$) closed-form stress solution can be developed for uniaxial compression [9],[10]. Based on the results the stress solutions of equibiaxial and volumetric compressions can also de defined.

In case of uniaxial compression the prescribed stretch history input is defined as

$$\lambda(t) = \begin{cases} 1+\dot{\varepsilon}t & t \le T \\ 1+\dot{\varepsilon}T & t > T \end{cases}, \tag{4.19}$$

which means that the body is compressed with constant $\dot{\varepsilon}$ strain rate in a finite $T$ time, then the strain is kept constant. This stretch function can be substituted back into the solution of the hyperelastic model in (4.5). Since in the visco-hyperelastic constitutive equation the deviatoric and hydrostatic part of the solutions are separated, the instantaneous stress response should also be splitted, therefore

$$\boldsymbol{\tau}_0^D(t) = \tau_0(t) \begin{bmatrix} \frac{2}{3} & 0 & 0 \\ 0 & -\frac{1}{3} & 0 \\ 0 & 0 & -\frac{1}{3} \end{bmatrix} = \sum_{i=1}^{N} \frac{2\mu_i}{\alpha_i}\left(\lambda^{\alpha_i}(t)-1\right) \begin{bmatrix} \frac{2}{3} & 0 & 0 \\ 0 & -\frac{1}{3} & 0 \\ 0 & 0 & -\frac{1}{3} \end{bmatrix}, \tag{4.20}$$

$$\boldsymbol{\tau}_0^H(t) = \frac{1}{3}\tau_0(t)\cdot\boldsymbol{I} = \sum_{i=1}^{N} \frac{2\mu_i}{3\alpha_i}\left(\lambda^{\alpha_i}(t)-1\right)\cdot\boldsymbol{I}, \tag{4.21}$$

where $\boldsymbol{I}$ is the second-order identity tensor. In the convolution integral the pull-back operator $\boldsymbol{F}_t(t-s)$ is also presented, which can be obtained using the relations in equations (4.19) and (3.14), thus

$$\boldsymbol{F} = \begin{bmatrix} \lambda(t) & 0 & 0 \\ 0 & 1 & 0 \\ 0 & 0 & 1 \end{bmatrix}, \qquad \boldsymbol{F}_t(t-s) = \begin{bmatrix} \frac{\lambda(t-s)}{\lambda(t)} & 0 & 0 \\ 0 & 1 & 0 \\ 0 & 0 & 1 \end{bmatrix}. \tag{4.22}$$

Since, both $\boldsymbol{\tau}_0^D(t)$ and $\boldsymbol{F}_t(t-s)$ tensors are diagonal, the order of the tensor product can be commuted, which leads that $\boldsymbol{F}_t(t-s)\,\boldsymbol{F}_t^{-1}(t-s) = \boldsymbol{I}$ can be simplified. Additionally, for diagonal tensors the SYM operator can also be simplified. Consequently, the convolution integral in (4.20) and 4.21) can also be simplified as

$$\begin{aligned} \boldsymbol{\tau}^D(t) &= \sum_{i=1}^{N}\frac{2\mu_i}{\alpha_i}\left(\lambda^{\alpha_i}(t)-1\right)\begin{bmatrix} \frac{2}{3} & 0 & 0 \\ 0 & -\frac{1}{3} & 0 \\ 0 & 0 & -\frac{1}{3} \end{bmatrix} \\ &\quad -\sum_{k=1}^{P}\frac{g_k}{\tau_k}\int_0^t\sum_{i=1}^{N}\frac{2\mu_i}{\alpha_i}\left(\lambda^{\alpha_i}(t-s)-1\right)\begin{bmatrix} \frac{2}{3} & 0 & 0 \\ 0 & -\frac{1}{3} & 0 \\ 0 & 0 & -\frac{1}{3} \end{bmatrix}\exp\left[-\frac{s}{\tau_k}\right]\mathrm{d}s, \end{aligned} \tag{4.23}$$

$$\boldsymbol{\tau}^H(t) = \sum_{i=1}^{N}\frac{2\mu_i}{3\alpha_i}\left(\lambda^{\alpha_i}(t)-1\right)\cdot\boldsymbol{I} - \sum_{k=1}^{P}\frac{g_k}{\tau_k}\int_0^t\sum_{i=1}^{N}\frac{2\mu_i}{3\alpha_i}\left(\lambda^{\alpha_i}(t)-1\right)\cdot\boldsymbol{I}\exp\left[-\frac{s}{\tau_k}\right]\mathrm{d}s. \tag{4.24}$$

These integrals could not be performed in one step, because $\lambda(t)$ and $\boldsymbol{\tau}_0(t)$ also consist of two parts: the uploading and the relaxation. Therefore, the hereditary integral is performed also in two steps and the closed-form stress response is provided by separated functions for the uploading and the relaxation, respectively. The input functions and the steps of the convolution integral are summarized in Fig. 4.5.

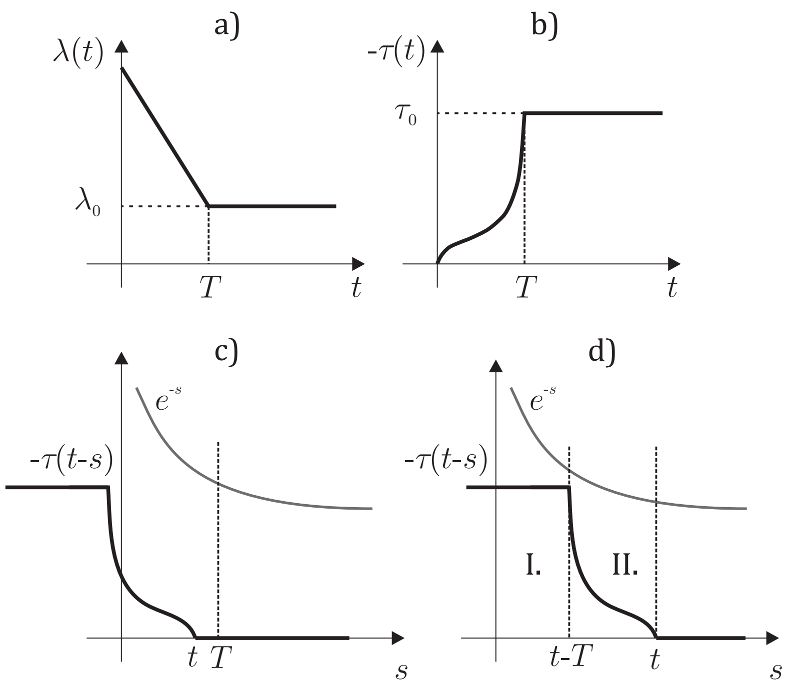


**Figure 4.5:** The prescribed a) stretch history input function $\lambda(t)$, b) the intantaneous stress response $\tau_0(t)$ and c)-d) the steps of the convolution integral for the uploading and the relaxation parts

### 4.2.1 Uploading part

In the uploading part, when $t \leq T$, after replacing $\lambda(t) = 1 + \dot{\varepsilon} t$ stretch input function into (4.23) and (4.24) and performing the integral, the stress response can be provided as

$$\begin{aligned} \boldsymbol{\tau}(t) &= \boldsymbol{\tau}^D(t) + \boldsymbol{\tau}^H(t) = \begin{bmatrix} \frac{2}{3} & 0 & 0 \\ 0 & -\frac{1}{3} & 0 \\ 0 & 0 & -\frac{1}{3} \end{bmatrix} \tau(t) + \begin{bmatrix} \frac{1}{3} & 0 & 0 \\ 0 & \frac{1}{3} & 0 \\ 0 & 0 & \frac{1}{3} \end{bmatrix} \tau(t) = \\ &= \begin{bmatrix} 1 & 0 & 0 \\ 0 & 0 & 0 \\ 0 & 0 & 0 \end{bmatrix} \tau(t), \end{aligned} \tag{4.25}$$

which means that the solutions satisfied the kinematic constrains for uniaxial compression. In the solution the $\tau(t)$ longitudinal principal stress becomes

$$\tau(t) = \tau_0(t) - \sum_{k=1}^{P} g_k \left( \sum_{i=1}^{N} \frac{2\mu_i}{\alpha_i} \eta_{ik} \right), \tag{4.26}$$

where, $\eta_{ik}$ can be directly calculated from the material and load parameters as

$$\eta_{ik} = \mathrm{e}^{-\frac{t}{\tau_k}} - 1 - \mathrm{e}^{-\frac{t+1/\dot{\varepsilon}}{\tau_k}} \left( -\frac{1}{\dot{\varepsilon}\tau_k} \right)^{-\alpha_i} \left( \Gamma\left[ 1+\alpha_i, -\frac{1}{\tau_k \dot{\varepsilon}} \right] - \Gamma\left[ 1+\alpha_i, -\frac{1+t\dot{\varepsilon}}{\tau_k \dot{\varepsilon}} \right] \right), \tag{4.27}$$

in which $\Gamma[a, z]$ is the so-called *incomplete upper gamma function*. By definition [20] [21], $\Gamma[a, z]$ is provided as

$$\Gamma[\nu, x] = \int_x^{\infty} t^{\nu-1} \mathrm{e}^{-t} \mathrm{d}t \tag{4.28}$$

Further detalis about the incomplete gamma function are summarized in *Appendix* C.

### 4.2.2 Relaxation part

During the relaxation part, when $t > T$, the stretch input $\lambda(t) = \lambda(T)$ is constant. This leads, that the instantaneous stress response $\boldsymbol{\tau_0}(t) = \boldsymbol{\tau_0}(T)$ is also constant. The convolution intagral can be performed as the sum of two integrals, namely

$$\boldsymbol{\tau}^D(t) = \boldsymbol{\tau}_0^D(T) - \sum_{k=1}^{P} \frac{g_k}{\tau_k} \left( \boldsymbol{\tau}_0^D(T) \int_0^{t-T} \exp\left[ \frac{-s}{\tau_k} \right] \mathrm{d}s + \int_{t-T}^{t} \boldsymbol{\tau}_0^D(t-s) \exp\left[ \frac{-s}{\tau_k} \right] \mathrm{d}s \right), \tag{4.29}$$

$$\boldsymbol{\tau}^H(t) = \boldsymbol{\tau}_0^H(T) - \sum_{k=1}^{P} \frac{g_k}{\tau_k} \left( \boldsymbol{\tau}_0^H(T) \int_0^{t-T} \exp\left[ \frac{-s}{\tau_k} \right] \mathrm{d}s + \int_{t-T}^{t} \boldsymbol{\tau}_0^H(t-s) \exp\left[ \frac{-s}{\tau_k} \right] \mathrm{d}s \right), \tag{4.30}$$

where firstly the integral on the $[0, t-T]$ interval defines the stresses related to the actual constant stretch value, while the integral on $[t-T, t]$ defines the remaining effect of the uploading part. The final form of the integral is the same as in (4.25), while solution of the longitudinal principal stress can be obtained as

$$\tau(t) = \tau_0(T) \left( 1 - \sum_{k=1}^{P} g_k \left( 1 - \exp\left[ -\frac{t-T}{\tau_k} \right] \right) \right) - \sum_{k=1}^{P} g_k \left( \sum_{i=1}^{N} \frac{2\mu_i}{\alpha_i} \vartheta_{ik} \right), \tag{4.31}$$

in which $\vartheta_{ik}$ depends on the parameters as

$$\vartheta_{ik} = \mathrm{e}^{-\frac{t}{\tau_k}} - \mathrm{e}^{-\frac{t-T}{\tau_k}} - \mathrm{e}^{-\frac{1+\dot{\varepsilon}t}{\dot{\varepsilon}\tau_k}} \left( \frac{-1}{\dot{\varepsilon}\tau_k} \right)^{-\alpha_i} \left( \Gamma\left[ 1+\alpha_i, \frac{-1}{\tau_k \dot{\varepsilon}} \right] - \Gamma\left[ 1+\alpha_i, \frac{-1-T\dot{\varepsilon}}{\tau_k \dot{\varepsilon}} \right] \right). \tag{4.32}$$

### 4.2.3 Summary

In the previous steps the stress solution for uniaxial compression was developed. Since, the equibiaxial and volumetric compressions are directly obtained form to the uniaxial compression using the relations in (4.8) and (4.11), the closed for solutions are also determined for equibiaxial and volumetric compressions as well. Therefore, the solution can be expressed as

$$\boldsymbol{\tau}_U(t) = \begin{bmatrix} \tau_0(t) & 0 & 0 \\ 0 & 0 & 0 \\ 0 & 0 & 0 \end{bmatrix}, \; \boldsymbol{\tau}_B(t) = \begin{bmatrix} \tau_0(t) & 0 & 0 \\ 0 & \tau_0(t) & 0 \\ 0 & 0 & 0 \end{bmatrix}, \; \boldsymbol{\tau}_V(t) = \begin{bmatrix} \tau_0(t) & 0 & 0 \\ 0 & \tau_0(t) & 0 \\ 0 & 0 & \tau_0(t) \end{bmatrix} \tag{4.33}$$

with

$$\tau(t) = \begin{cases} \tau_0(t) - \sum\limits_{k=1}^{P} g_k \left( \sum\limits_{i=1}^{N} \dfrac{2\mu_i}{\alpha_i} \eta_{ik} \right) & t \leq T \\ \tau_0(T) \left( 1 - \sum\limits_{k=1}^{P} g_k \left( 1 - \exp\left[ -\frac{t-T}{\tau_k} \right] \right) \right) - \sum\limits_{k=1}^{P} g_k \left( \sum\limits_{i=1}^{N} \dfrac{2\mu_i}{\alpha_i} \vartheta_{ik} \right) & t > T \end{cases} \tag{4.34}$$

where $\boldsymbol{\tau}_U, \boldsymbol{\tau}_B$ and $\boldsymbol{\tau}_V$ denotes the uniaxial, the equibiaxial and the volumetric compressions, respectively. This closed-form solutions can be utilized in the parameter-fitting process, where the more accurate fitting approach can be applied based on the uniaxial stress solution of open-cell polymer foams.

# 5 Measurements

The accurate the finite element analysis of polyer foams requires to obtain the material parameters in the visco-hyperelastic material model (3.19 and 3.20), which can be determined via parameter-fitting based on measurement data. In accordance with the main fields of application, where the load is dominantly compression, uniaxial compression test were performed on the investigated memory foam material.

The goal of the measurement is to investigate experimentally the viscoelastic material behaviour and to provide measurement data for the parameter fitting process. As a result, the stress-strain characteristics corresponding to different load cases are obtained, which also present the most significant viscoelastic phenomena, namely as the strain rate dependency, the hysteresis and the stress relaxation.

## 5.1 Introduction

The measurements were performed in the laboratory of the Department of Applied Mechanics with an INSTRON 3345 Single Colum Universal Testing System. The load was measured by an INSTRON model 2519-107 5kN load cell. In order to increase the cross section of the specimens an additional compression platen were mounted to the system. The measurement layout is presented in Fig. 5.1.

During experimental investigation of the time-dependent material behavior, the following two compression tests were performed:

1. Relaxation test
2. Cyclic test with incremental loading

In both test the $u(t)$ displacement was controlled, while the load $F$ was the output, the sampling interval was 0.01 s. The measurement were performed under similar environmental conditions namely 22°C air temperature and 44% relative humidity.

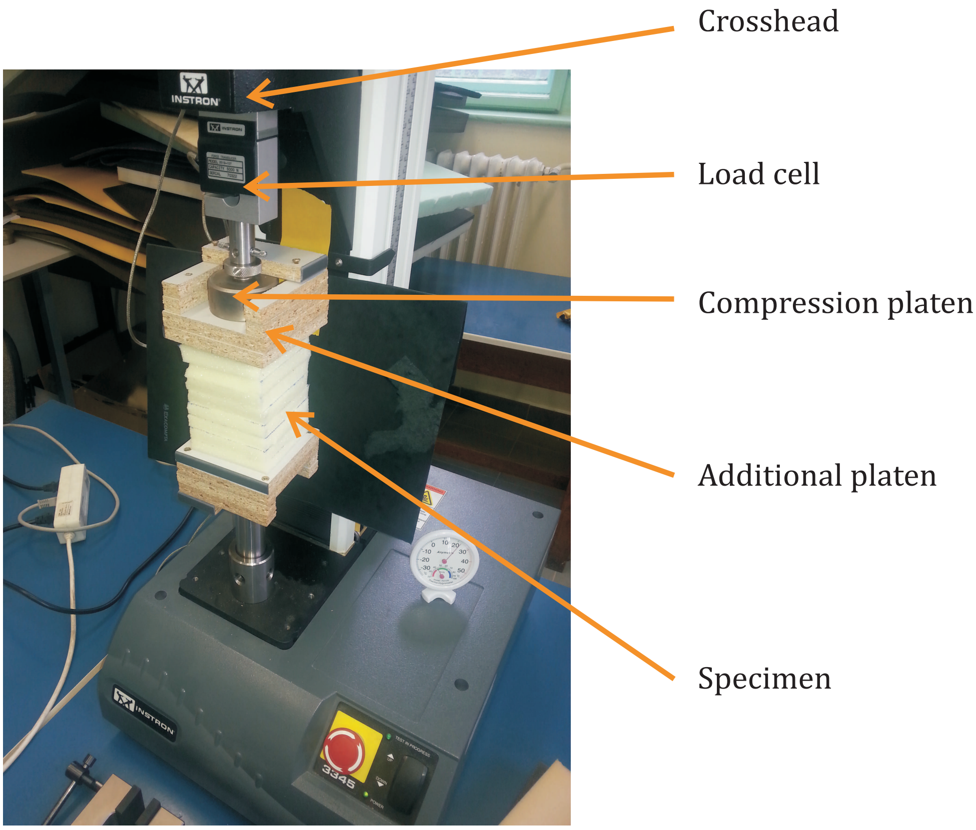


**Figure 5.1:** The layout of the measurement using INSTRON Testing System

### 5.1.1 Specimens

The investigated memory foam is a commercial polyurethane foam, distributed by Csomaeszk Kft in Hungary. The "*Memoryszivacs*" memory foam sheet is applied in mattrasses and medical products. The memory foam is sold in the size of $200 \times 160 \times 1$.

The specimens for the compession test were cutted from the raw material sheet. The specimens were created accordingly to the international standard of ISO-3386-1 [22]. The standard requires the specimens to be right parallelepiped with a minimum width/thickness ratio of 2:1. The optimal thickness is 50 mm, although when the specimens are thinner, the longitudinal length ($L_0$) can be heightened by plying specimens together. Additionally, it is recommeded that the cross section should the as large as possible, but it should not overlap the compression platen. Based on the recommendations in the standard the size of the specimens became $8 \times 8$ cm and 8 piece of them were plied together. The dimensions of the specimens are listed in Table 5.1, while its geometry is presented in Fig. 5.2.

| Material | Polyurethane |
|---|---|
| Thickness ($t$) | 10 mm |
| Width of the specimen ($w$) | 80 mm |
| Cross section ($A_0$) | 6400 mm$^2$ |

**Table 5.1:** The dimensions of the specimens

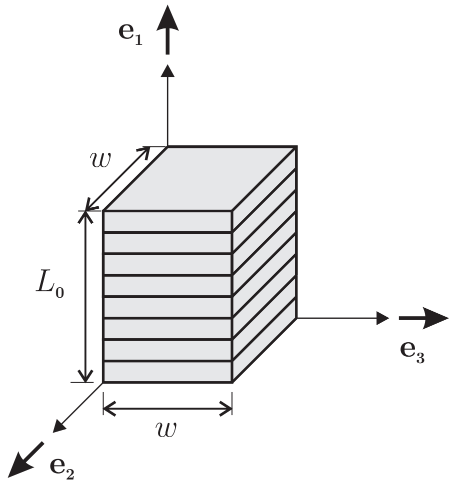


**Figure 5.2:** The geometry of specimens

### 5.1.2 Evaluation of measurements

During the measurements in every sampling point the corresponding load ($F$) and displacement ($\Delta L$) values were recorded. The initial separation of the platens $H_0 = 110$ mm is bigger, than the height ($L_0$) of the specimen. Therefore, at the beginning of the measured load is zero, since the platens to not touch the specimens. The actual starting point can be obtained by utilizing the so-called *slack correction* method, which is presented in Fig. 5.3.

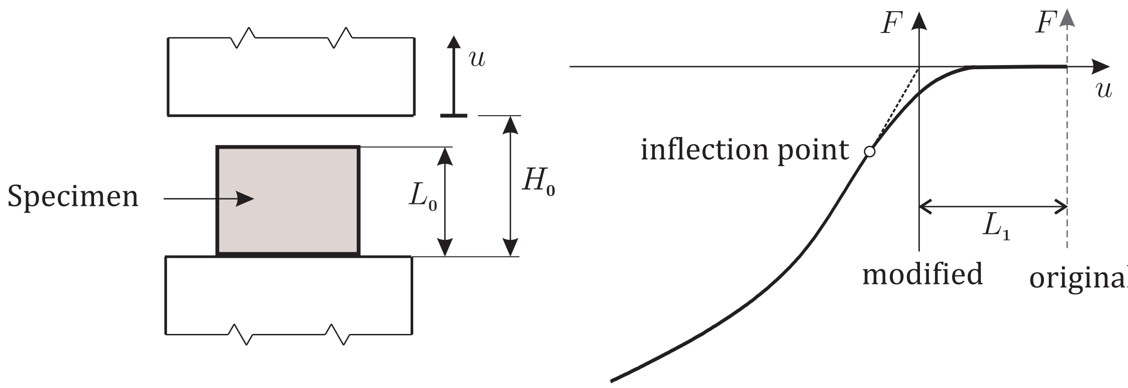


**Figure 5.3:** The measurement layout and the slack correction method

Due to the specimen plying, in the initial region of the measured $F - \Delta L$ characteristic an inflection point can be detected. This error can be corrected with the tangent line from the inflection point, which also determined the $L_1$ displacement corresponding to the starting point. Using this $L_1$ displacement value, the exact height of the specimen can be calculated as

$$L_0 = H_0 - L_1 \tag{5.1}$$

From the measured $F - \Delta L$ data, the longitudnial stretch ($\lambda_1$) and the stress ($P_1$) data can be obtained as

$$\lambda_1 = 1 + \frac{u}{L_0}, \qquad P_1 = \sigma_1 = \frac{F}{A_0}, \tag{5.2}$$

where the Cauchy and the 1st Piola–Kirchhoff stresses are identical, since the transversal (or cross-directional) strains can be neglected according to the assumption in (2.30), i.e. $\lambda_T = 1$.

It should be noted, that due to the small sampling time (0.01 s), the measurement results (data points) can be illustrated with continous curves.

## 5.2 Relaxation test

The time-dependent material behaviour can be characterised by the stress relaxation phneomena (see *Section* 3.1), which can be investigated in ideal case as the stress response for unit step strain input. In real measurement it means infinite strain rate at $t = 0$, therefore it is well-known that only ramp test can be performed. In this case, the specimen is compressed with constant strain rate in a finite $T$ time and then the strain is kept constant, while the stress relaxes. In order to have significant relaxation, the uploading strain rate ($\dot{\varepsilon}$) should be as high as possible. During the performed test on the investigated memory foam the crosshead speed was the highest possible, namely $v = 1000$ mm/min, for the maximal strain $u_{\max} = 85$ mm and for the relaxation time 600 s were prescribed. The displacement input of the relaxation test is presented in Fig. 5.4.

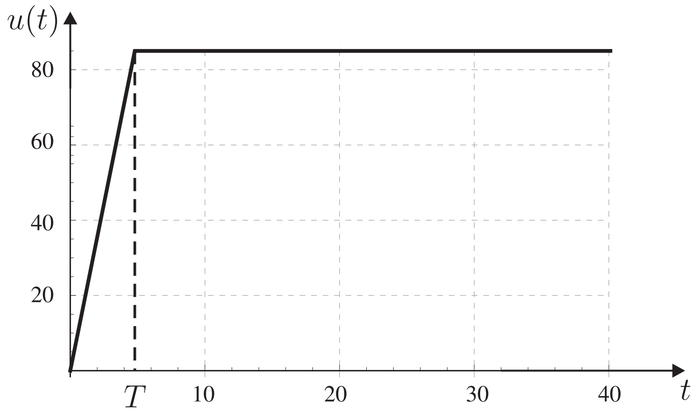


**Figure 5.4:** The prescribed time-history of the displacement in case of the relaxation test

The time of uploading ($T$), the maximal longitudinal stretch ($\lambda_{\max}$) and the strain rate ($\dot{\varepsilon}$) are determined from the exact dimensions of the specimen obtained from equation (5.1). The parameters of the relaxation test are listed in Table 5.2.

| | |
|---|---|
| Time of uploading ($T$) | 4.792 s |
| Maximal longitudinal stretch ($\lambda_{\max}$) | 0.240198 |
| Strain rate ($\dot{\varepsilon}$) | $-0.1585565$ 1/s |
| Exact height of the specimen ($L_0$) | 104.082 mm |

**Table 5.2:** The parameters of the relaxation test

### 5.2.1 Results

The result of the measurement and the stress relaxation phenomena can be presented by the Cauchy stress-time ($\sigma - t$) and the Cauchy stress- stretch ($\sigma - \lambda$) characteristics, which are presented in Figs. 5.5 and 5.7.

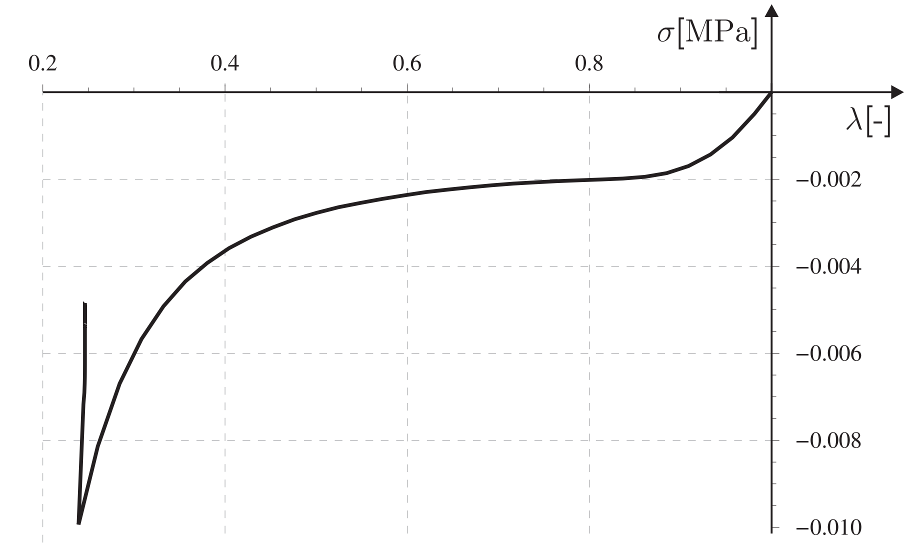


**Figure 5.5:** The stress-stretch characteristic $(\sigma - \lambda)$ in case of the relaxation test

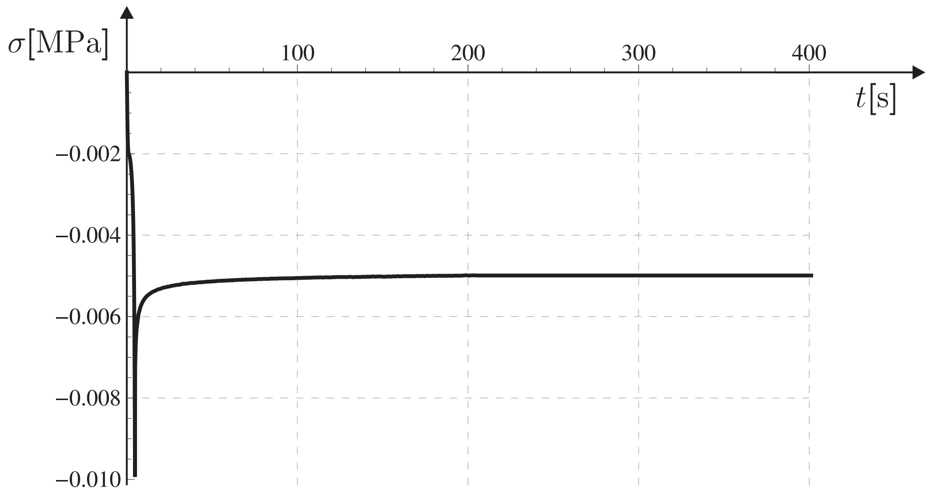


**Figure 5.6:** The stress response on the $t \in [0, 400]$ domain in case of relaxation test

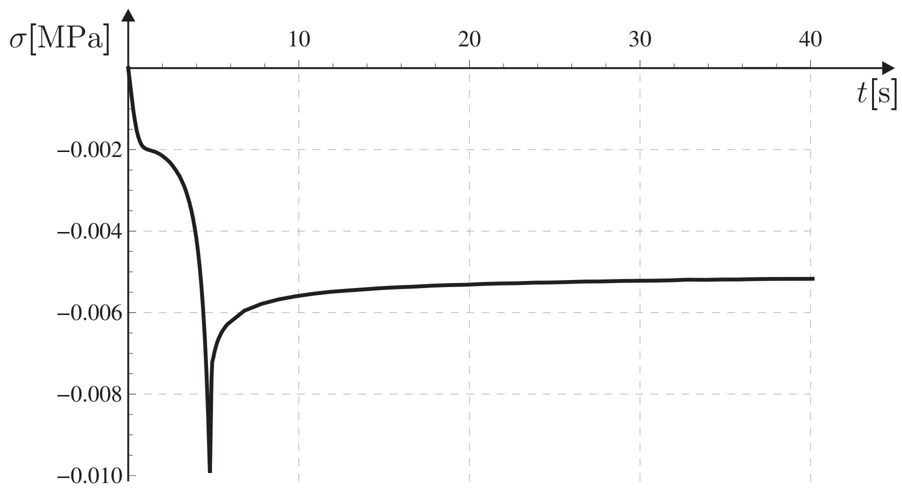


**Figure 5.7:** The stress response on the $t \in [0, 40]$ domain in case of relaxation test

The characteristics shows, that the investigated memory foam shows significant viscoelacatic properties, therefore our approach, which states that this particular material should be modelled using visco-hyperelastic material models, is verified.

## 5.3 Cyclic test

Beside the relaxation test, the viscoelastic behaviour of the memory foram can be inveastigated via cyclic test. During this test the specimen is compressed incrementally with low strain rate in a way, that after every strain increment the strain kept constant and the stress relaxed. Similarly, the downloading process is perfromed in increments. Due to the viscoelastic properties, the uploading and the downing process follows different pathes due to the energy dissipation in the material. During the relaxation, the stress values tends to the long-term (time-independent) stress response, thus the results of the cyclic test can be applied in the parameter-fitting of the time-independent hyperelastic material model.

In case of the cyclic test the dispalcement increment was set $\Delta u = 8{,}5$ mm, the crosshead speed was $v = 100$ mm/min, while the relaxation intervals were $t_{REL} = 30$ s. The prescribed displacement-history input funtion is presented in Fig. 5.8. The exact values of the strain rate ($\dot{\varepsilon}$) and the strain increment ($\Delta\varepsilon$) can be calculated from the height of the specimen obtained in (5.1). Table 5.3 presents the measurement parameters.

| Parameters | |
|---|---|
| Maximal longitudinal stretch ($\lambda_{\max}$) | 0.23183 |
| Strain rate ($\dot{\varepsilon}$) | $-0.01546$ 1/s |
| Strain increment in the first step ($\Delta\varepsilon_0$) | 0.0723 |
| Strain increment ($\Delta\varepsilon$) | 0.0773 |
| Exact height of the specimen ($L_0$) | 107.835 mm |

**Table 5.3:** The parameters of the cyclic test

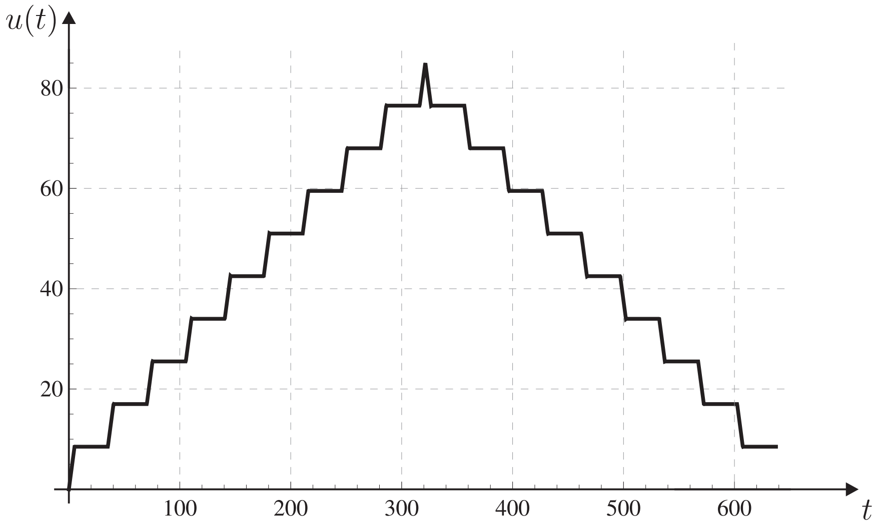


**Figure 5.8:** The prescribed time-history of the displacement in case of the cyclic test

### 5.3.1 Results

The results of the cyclic test can be summarized by the Cauchy stress-time ($\sigma - t$) and the Cauchy stress-stretch ($\sigma - \lambda$) characteristics, which are provided in Figs. 5.10 and 5.9. The results show, that the relaxation is significant in this loading case as well, when the applied rate of deformation was lower. Additionally, the time-dependent behavior can be also represented by the $\sigma - \lambda$ curve, where a hysteresis can be found, which reflects to the energy dissipated in the material.

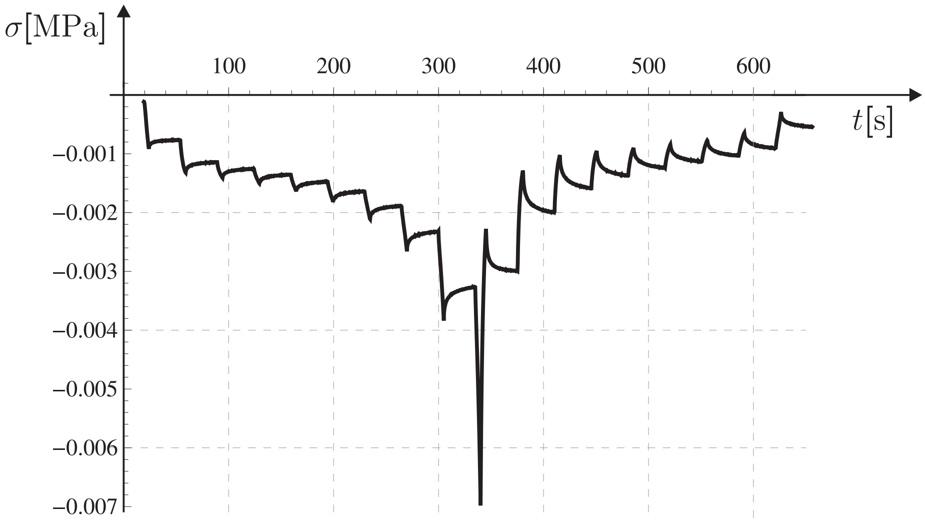


**Figure 5.9:** The stress response in case of the cyclic test

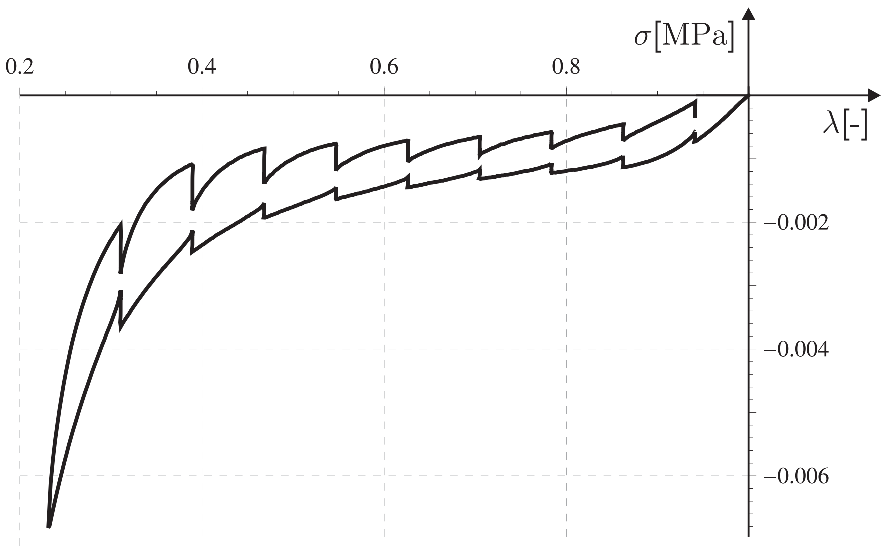


**Figure 5.10:** The stress-stretch characteristic ($\sigma - \lambda$) in case of the cyclic test

## 5.4 Summary of the measurement results

The results of the performed uniaxial compression tests demonstate the time-dependent viscoelastic properties of the memory foam material. The results can be summarized on a common $\sigma - \lambda$ stress-stretch diagram (see Fig. 5.11). These characteristics show that the stress values in case of the relaxation test are higher than the stress values obtained by cyclic test, since the strain rate were also higher in case of the relaxation test. Additionally, it can be clearly seen, that in the relaxation regions of both tests the stress values tends to the long-term (time-independent) stress response values, which lay inbetween the up- and downloading parts of the cyclic test.

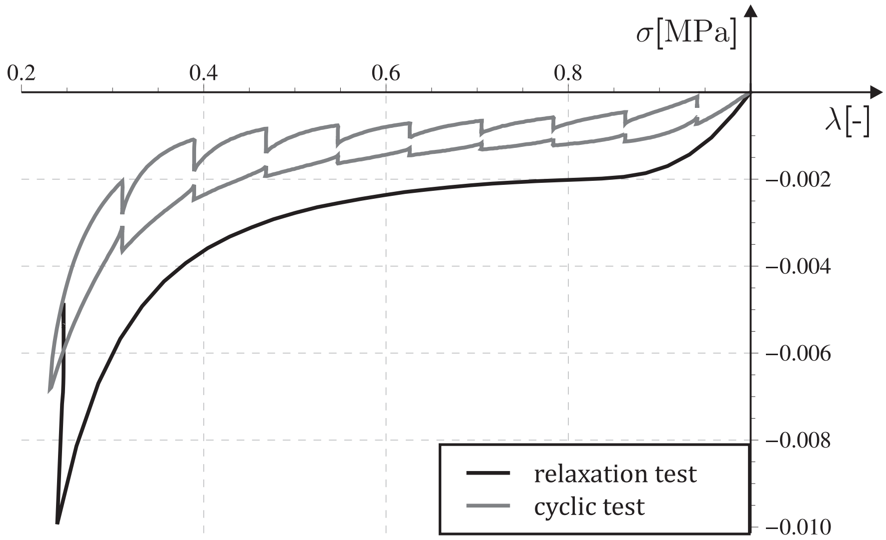


**Figure 5.11:** The measured stress-stretch characteristics ($\sigma - \lambda$) in case of two different uniaxial compression tests

As the measurement results show, the material bahaviour of the memory foam requires visco-hyperelastic material modelling approach. Additionally, the recorded characteristics provides the sufficient data for the further parameter fitting process.

# 6
# Parameter fitting

The parameter fitting is the last step in the material modelling process. In this step the material parameters are determined, which are included in the constitutive equation describing the material behaviour. Based on the fitted material parameters the mechanical response could be investigated in case of complex load cases using finite element analysis. Although, it should be emphasized that the results of the finite element analysis are very sensitive to the material parameters both qualitatively and quantitatively. Therefore, the material parameters should be fitted as accurately as possible. Otherwise the results of the finite element analysis could be inaccurate.

The parameter fitting method is based on the analytical solution corresponding to the measured load case. In case of the visco-hyperelastic material model, this analytical solution is not available, therefore an alternative, so-called separated method is applied in the literature. However, the closed-form stress solutions for uniaxial compression is derived in *Section* 4, thus the entire material model can be fitted in one-step. This latter method provides a better solution for the parameters, thus the finite element analysis will be more accurate [9],[10].

## 6.1 The method of parameter fitting

During the parameter fitting process the analytical solution of the material model is fitted to measurement data points. Nevertheless, several methods are provided in the literature for the parameter fitting process. The least square fitting technique is the most commonly applied method, where the global extremum of the error function is searched in $\mathbf{p}$, the space of the unknown parameters. In this method the error function is defined as

$$e = \sum_{i=1}^{N} \left[ f^A(x_i, \mathbf{p}) - f^M(x_i) \right]^2 , \tag{6.1}$$

where $N$ is the number of measurement data points, $f^A$ the analitical function to be fitted, $x_i$ the values of the independent variable at the measurement points, while $f^M(x_i)$ denotes the measured values at the measurement points. This multidimensional global extreme-value problem cannot be solved analytically, therefore numerical methods have to be applied [2]. During my calculations the `"NMinimize"` algorithm was applied, which is a bulit-in algorithm in Wolfram Mathematica[23]. The algorithm finds the global minimum of a multidimensional function using deterministic and stochastical methods. The available stochastical methods, which are referred as `"SimulatedAnnealing"`, `"NelderMead"` and `"RandomSearch"`, search for the global minimum from random points in the parameter space. The only available deterministic method, the `"DifferentialEvolution"`, follows the local gradient of the function to be minimized. It should be noted, that there is not any general method, which finds the minimum in the best and most effective way. The results of the extreme-value problem always depends on the function to be minimized, futhermore it is common that the different methods provide different results for the same problem [23].

In case of the investigated memory foam material, the goal of the parameter fitting method is to determine both the viscoelastic and the hyperelastic parameters as it is provided in (4.34) based on the measurement data of the stress relaxation test. The number of material parameters included in the visco-hyperelastic model are: $2N$ $(\alpha_1, \alpha_2 ... \alpha_N; \mu_1, \mu_2 ... \mu_N)$ parameters for the time-independent hyperelastic model and $2P$ $(g_1, g_2 ... g_P; \tau_1, \tau_2 ... \tau_P)$ parameters for the time-dependent viscoelastic model. It means that altogether $2(N + P)$ parameters should be fitted to our measurement data in order to describe the visco-hyperelastic material behavior.

## 6.2 Parameter fitting algorithms in case of visco-hyperelastic materials

In case of visco-hyperelastic material model the parameter fitting is even more complicated since the exact stress solution should be obtained as the solution of the convolution integrals in (3.19) and (3.20). In the literarure closed-form solution for the *Hyperfoam*-based visco-hyperelastic model has not been published yet for any load case. Therefore, an alternative parameter fitting method is adopted, which is called as *separated* fitting [8].

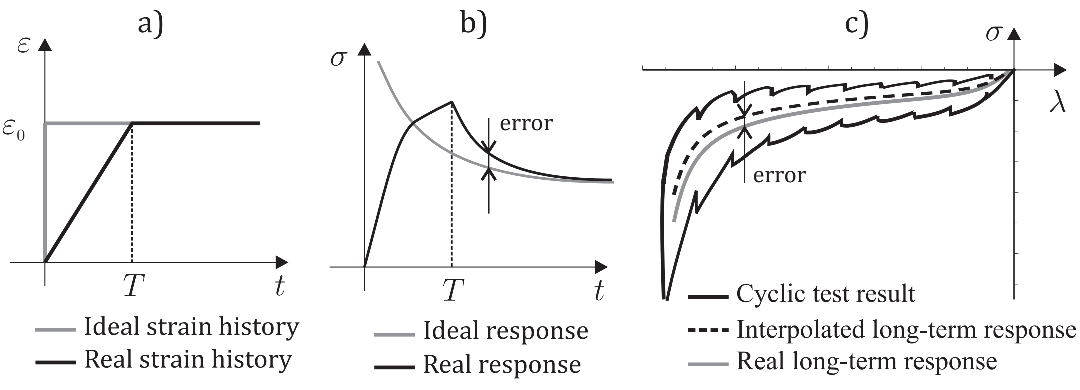


**Figure 6.1:** The applied a) stretch input and the b)-c) fitting errors induced during the separated fitting method

The concept of this algorithm is to find the parameters for a visco-hyperelastic material by separating the parameter fitting of the long-term behaviour and the time-dependent stress relaxation. In this approach the hyperelastic model is fitted to the long-term stress response, while the viscoelastic parameters are fitted to the stress relaxation behaviour. The long-term behavior is determined from cyclic compression-relaxation loading (see Fig. 5.9), where the data points corresponding to the long-term behavior appears between the uploading and downloading curves. The data points could be determined using interpolation from the corresponding stress minima and maxima, usually as the mean value. This induces errors in the parameter fitting process. Additionally, it is assumed that the stress relaxation test is performed using step loading. However, it is well-known that in real measurements ramp loading is used instead of step loading, which induces significant error in the fitted viscoelastic parameters. The fitting errors included during the separated method are summarized and presented in Fig. 6.1, [7], [6].

In order to fit accurately the material model, it is essential to obtain the stress solution for the ramp loading. Then, the entire material model can be fitted to the experimental data without separating the long-term behavior and the relaxation behavior. In the literature the closed-form stress solution is provided only for simpler, usually incompressible visco-hyperelastic material models. The solution for the *Hyperfoam*-based model is not available, therefore this fitting method has not been applied, yet. However, in *Chapter* 4 the analytical stress solution was derived for uniaxial compression, therefore this makes it possible to apply the closed-form fitting approach in case of the open-cell polymer foams as well.

## 6.3 Separated fitting of parameters

In the process of the separated fitting, the material parameters of the long-term (rate-independent) stress response and the time-dependent stress relaxation behaviour are fitted separately using different measurement data. The material parameters of the long-term hyperelastic material model denoted as $(\tilde{\alpha}_i, \tilde{\mu}_i)$, while the stress relaxation is characterized using the Prony-parameters $(g_i, \tau_i)$. It should be noted, that the long-term hyperelastic parameters $(\tilde{\alpha}_i, \tilde{\mu}_i)$, are not equal with the hyperelastic parameters $(\alpha_i, \mu_i)$ in the visco-hyperelastic constitutive equation in (3.19) and (3.20), which were related to the instantaneous stress response. However, the long-term and the instantaneous stress responses can be related as

$$\tau_0(t) = \frac{1}{g_\infty}\tau_\infty(t) \tag{6.2}$$

where $g_\infty = 1 - \sum g_i$ can be obtained from the $g_i$ time-dependent Prony-parameters. In Abaqus [5] the hyperelastic parameters can be defined both for the long-term and the instantaneous stress responses, thus it does not induce any further error during the fitting process.

### 6.3.1 Hyperelastic parameters

In order to fit the long-term hyperelastic parameters, the data points corresponding to the long-term stress response should be determined. This can be related to the results of the cyclic test (see Fig. 5.9). The relaxation parts of the cyclic test tend to the long-term stress response values, therefore in "infinite" time the required measurement points could be reached. Nevertheless, the relaxation was finite in time, thus the stress values did not reached the long-term stress values. To obtain the corresponding data points, firstly the local extremums were detected (the stress values at the end of each relaxation session) and then, using linear interpolation, the data points could be determined. In case of the measured memory foam material altogether 10 point could be defined, which corresponds to the long-term stress response and for which the hyperelastic material model can be fitted. The resulted data points are shown in Fig. 6.2. In the fitting process a second-order hyperelastic material model was applied, i.e. $N = 2$. Based on equation (4.5), the function to be fitted becomes

$$\tau_1 = \frac{2\tilde{\mu_1}}{\tilde{\alpha_1}} \left(\lambda_1^{2} - 1\right) + \frac{2\tilde{\mu_2}}{\tilde{\alpha_2}} \left(\lambda_1^{2} - 1\right), \tag{6.3}$$

which contains 4 material parameters, namely $\tilde{\alpha_1}, \tilde{\alpha_2}, \tilde{\mu_1}, \tilde{\mu_2}$. As it was derived previously in (2.37), the parameters should satisfy the following criterium:

$$\tilde{\mu_1} + \tilde{\mu_2} > 0. \tag{6.4}$$

The parameter fitting was performed in Mathematica using the built-in `NMinimize` algorithm, in which the corresponding error function (introduced in 6.1) was obtained as

$$\bar{e} = \sum_{i=1}^{N} \left[ \left( \frac{2\tilde{\mu_1}}{\tilde{\alpha_1}} \left(\lambda_1^{2} - 1\right) + \frac{2\tilde{\mu_2}}{\tilde{\alpha_2}} \left(\lambda_1^{2} - 1\right) \right) - P_i^M \right]^2 \tag{6.5}$$

The results of the parameter fitting is presented in Fig. 6.2, while the fitted parameters are listed in Table 6.1.

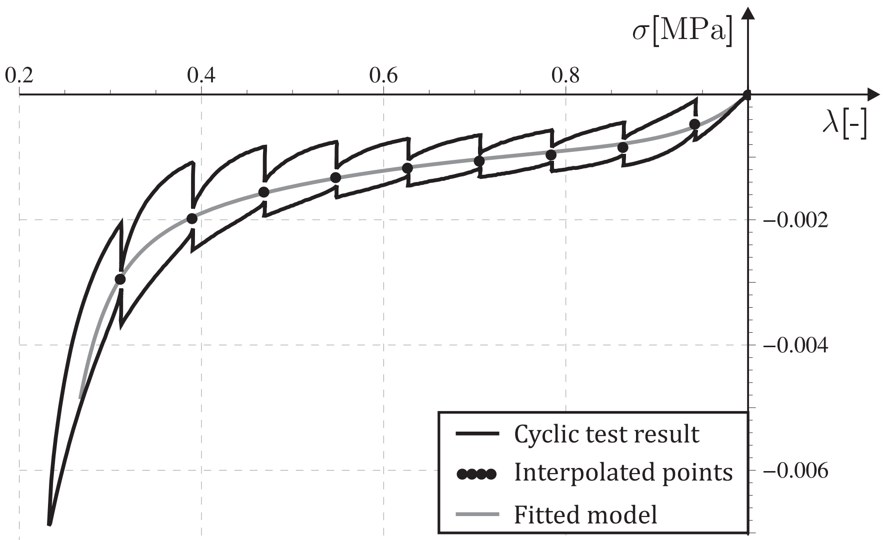


**Figure 6.2:** The fitted hyperelastic material model using separated fitting methof

| Hyperelastic parameters | $\tilde{\alpha_1}$ | $\tilde{\alpha_2}$ | $\tilde{\mu_1}$ | $\tilde{\mu_2}$ |
|---|---|---|---|---|
| | $-7{,}2397$ | 18,3649 | $1{,}417\ 10^{-7}$ | 0,00669 |

**Table 6.1:** The hyperelastic parameters using separated fitting method

The hyperelastic parameters can also be determined with the built-in fitting algorithm in Abaqus. In this case, the obtained material parameters are listed in Table 6.2.

| Hyperelastic parameters | $\tilde{\alpha_1}$ | $\tilde{\alpha_2}$ | $\tilde{\mu_1}$ | $\tilde{\mu_2}$ |
|---|---|---|---|---|
| | $-6{,}70459$ | 19,776 | $2{,}51455\ 10^{-7}$ | 0,00715936 |

**Table 6.2:** The hyperelastic parameters fitted in Abaqus

If we compare the results with the previously defined parameters in Table 6.1, it can be seen that there is no significant difference. Therefore, during the further calculations those parameters will be applied, which were fitted by the numerical algorithm in MATHEMATICA.

The material parameters should also satisfy the Drucker-stability criteria defined in equations (2.49)-(2.51). The stability was checked in ABAQUS, where the results were exported into the `Job.dat` file. The results of the stability analysis are listed in Table 6.3.

| Load case | Stability |
|---|---|
| Uniaxial tension | Stable for all strains |
| Uniaxial compression | Stable for all strains |
| Biaxial tension | Stable for all strains |
| Biaxial compression | Stable for all strains |
| Volumetric tension | Stable for all volume ratios |
| Volumetric compression | Stable for all volume ratios |
| Simple shear | Stable for all shear strains |

**Table 6.3:** The stability of the hyperelastic model in case of separated fitting method

As the results shows, the fitted hyperelastic model is stable for all deformations.

### 6.3.2 Prony parameters

The time-dependent viscoelastic behavior is characterized by the Prony-parameters (see equation 3.15), which can be fitted to the relaxation test results (see Fig. 5.6). The measurement results are considered to be ideal relaxation response corresponding to step loading, in this case the stress solution becomes

$$\sigma(t) = E_0 \left( e_\infty + \sum_{k=1}^{P} e_k \exp\left[\frac{-t}{\tau_k}\right] \right) \varepsilon_0 \tag{6.6}$$

This yields, that the time-dependent relaxation modulus $E(t)$ can be expressed as

$$E(t) = \frac{\sigma(t)}{\varepsilon_0} = E_0 \left( e_\infty + \sum_{k=1}^{P} e_k \exp\left[\frac{-t}{\tau_k}\right] \right), \tag{6.7}$$

which can be also obtained from the measurement data. The relation that $e_\infty E_0 = E_\infty$ gives

$$E(t) = \frac{E_\infty}{e_\infty} \left( e_\infty + \sum_{k=1}^{P} e_k \exp\left[\frac{-t}{\tau_k}\right] \right), \tag{6.8}$$

where $E_\infty$ is calculated as the limit of the $E(t)$, in our case $E_\infty = 0.00643$ MPa. Dividing equation (6.8) with the calculated $E_\infty$ value and expressing $e_\infty$ based on (3.16), the the function $\bar{E}(t)$ , which should be fitted to the measurement data, becomes

$$\bar{E}(t) = \frac{E(t)}{E_\infty} = \frac{1}{1 - \sum_{k=1}^{P} e_k} \left( 1 - \sum_{k=1}^{P} e_k + \sum_{k=1}^{P} e_k \exp\left[\frac{-t}{\tau_k}\right] \right), \tag{6.9}$$

where the unknown material parameters are $e_k$ and $\tau_k$. The so-called relaxation moduli can be described with the same parameters, this yields that $e_k = g_k = k_k$. Therefore, using the notation of the visco-hyperelastic material model, the $\bar{E}(t)$ function is obtained as

$$\bar{E}(t) = \frac{1}{1-\sum_{k=1}^{P} g_k}\left(1-\sum_{k=1}^{P} g_k+\sum_{k=1}^{P} g_k \exp\left[\frac{-t}{\tau_k}\right]\right). \tag{6.10}$$

The same transformation should be performed on the measurement data as well. Firstly, the stress relaxation function ($\sigma - t$) was divided with the corresponding strain $\varepsilon_0 = -0{,}7598$, then the long-term elastic modulus was obtained from $E_\infty = 0{,}00643$ MPa. After dividing the measurement data with $E_\infty$, the function in (6.10) can be fitted. For the order of the Prony series, $P = 3$ was chosen and the fitting criteria $\tau_k > 0$, $g_k > 0$, $g_1 + g_2 + g_3 < 1$ were defined. The fitting was performed using the `NMinimize` built-in MATHEMATICA algorithm. The result of the parameter fitting is presented in Fig. 6.3, while the corresponding material parameters are listed in Table 6.4.

| Prony parameters | $g_1$ | $g_2$ | $g_3$ | $\tau_1$ | $\tau_2$ | $\tau_3$ |
|---|---|---|---|---|---|---|
| | 0,61213 | 0,03739 | 0,01586 | 2,3221 | 20,6702 | 242,424 |

**Table 6.4:** The fitted Prony-parameters using separated fitting method

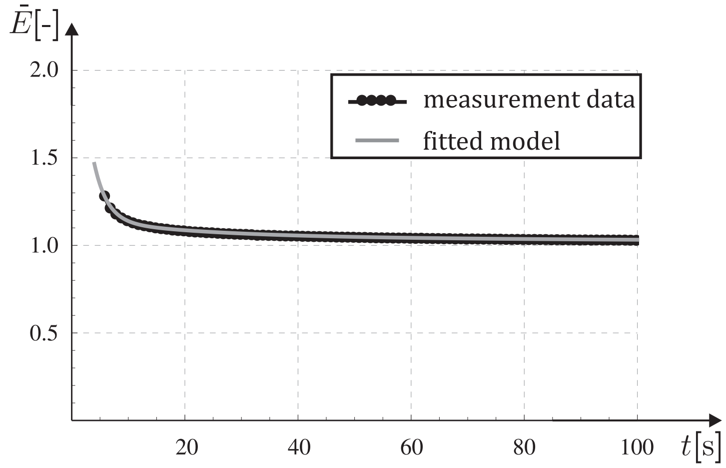


**Figure 6.3:** The time dependent modified elastic modulus $\bar{E}(t)$ and the fitted model using Prony-series

It should be noted, that for the viscoelastic parameters there is no available built-in fitting algorithm in ABAQUS, thus the parameter fitting can be performed using own fitting algorithm.

### 6.3.3 Validation with FEA

In the previous two subsections all material parameters have been identified in the visco-hyperelastic constitutive equation using two separated algorithms for the hyperelastic and the viscoelastic parameters. The fitted mechanical model can be validated using finite element analysis (FEA). The goal of the analysis is to investigate the accuracy of the fitted model based on real measurement data. During the FEA, the relaxation test was analysed.

The geometry is an eighth model with unit cube, on which the same strain input was applied as in case of the real measurement (see. Fig. 5.4). The mesh containes only one eight-node brick element with reduced integration (C3D8R). On nodes 1-4 zero for all diplacements $U_{1,2,3} = 0$ was prescribed, while on nodes 5-8 for the cross-directional displacements $U_{2,3} = 0$ was applied. Based on the relaxation test data the longitudinal displacement was $U_1 = 0{,}7598$ mm, while the time of uploading was $T = 4{,}792\,\mathrm{s}$. The geometry of the FE model and the boundary conditions are presented in Fig. 6.4.

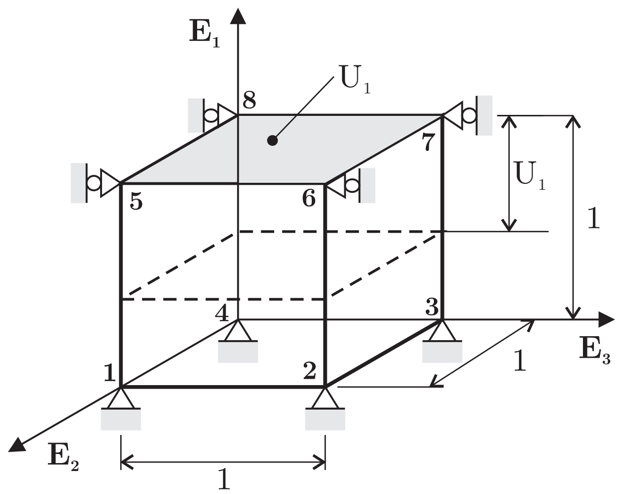


**Figure 6.4:** The finite element model and the applied constraints

The FEA was divided into two steps. In the first step the body is compressed with constant strain rate, while in the second step the stain is kept constant, thus the stress could relax. The steps were computed in defined increments in order to provide accurate numerical solution for the nonlinear material model. The parameters of the steps applied during the FEA are listed in Table. 6.5.

| Step | Start | End | *Increment* | Number of *Increments* |
|---|---|---|---|---|
| Step 1 | 0 s | 4.792 s | 0.01 s | 480 |
| Step 2 | 4.792 s | 100 s | 0.2 s | 500 |

**Table 6.5:** The parameters of the FEA

As the result of the analysis the principal longitudinal stress ($\sigma_1$) and the strain ($\varepsilon_1$) values were queried from node 6 for all increments, which provides all necessary information for the validation of the material model.

### 6.3.4 The results of the separated fitting

The results of the FEA, in which the fitted material model was applied, can be compared with the measurement results of the relaxation test, which is presented in Fig. 6.5. As the result shows, in the uploading part the fitted material model is close to the real measured data, while in case of the stress relaxation part the error is significant. This can be explained by the approximation that was applied during the fitting of stress relaxation, namely the relaxation data corresponds to the ideal step load input. Addionally, the interpolation and the limited data points of the long-term hyperelastic response also induces errors. It should be emphasized that in the literaute there are several methods, which can reduce the errors in the Prony-parameters by modifying the experimental data according to the method proposed by Zapas and Phillips [24], for instance. But, these methods requires further calculations and data manipulations.

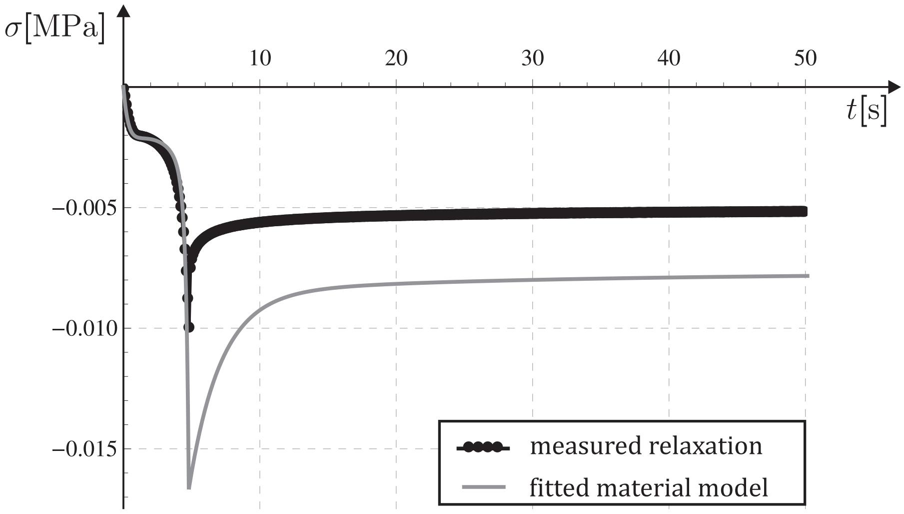


**Figure 6.5:** The comparison of the measured data with the fitted material model in case of separated method

## 6.4 Closed-form parameter fitting

As the results of the separated fitting method shows, the material model will be inaccurate if the parameters are fitted separately. Moreover, the inaccurate material model cause serious errors during the FEA, which means that the calculated material behaviour differs significantly from the real material response. In order to minimize the fitting errors, the material parameters should be fitted in one-step using the closed-form stress solutions. This solution was derived for the investigated memory foam material, when the loading is uniaxial compression. By adopting the stress solution in (4.34) all the $2N$ $(\alpha_1, \alpha_2 ... \alpha_N; \mu_1, \mu_2 ... \mu_N)$ hyperelastic and the $2P$ $(g_1, g_2 ... g_P; \tau_1, \tau_2 ... \tau_P)$ time-dependent Prony parameters can be identified simultaneously. This method increases the computation time, but the fitted material parameter characterize the visco-hyperelastic material behaviour more accurately [9],[10].

### 6.4.1 Identification of material parameters

Since the closed-form stress response $\tau(t)$ is obtained in equation (4.34), the material model can be fitted directly to the stress relaxation data (see Fig. 5.6). The parameters of the loading case were the strain rate $\dot{\varepsilon} = -0.1585565$ 1/s and the time of uploading $T = 4{,}792\,\mathrm{s}$. The parameter fitting was performed again in Mathematica using the `NMinimize` global minimizer algorithm, where the error function (to be minimized) was defined as

$$e = \frac{1}{N_1} \sum_{i=1}^{N_1} \left[ \tau\left(t_i^{M_1}\right) - \sigma_i^{M_1} \right]^2 + \frac{1}{N_2} \sum_{i=1}^{N_2} \left[ \tau\left(t_i^{M_2}\right) - \sigma_i^{M_2} \right]^2, \tag{6.11}$$

where $N_1$ and $N_2$ denotes the measurement points in the uploading and the stress relaxation parts, respectively. The applied material model contains a second-order hyperelastic ($N = 2$) and a third-order Prony-series ($P = 3$).

Based on the conditions in (2.37), the criteria for the parameters were defined as

$$\mu_1 + \mu_2 > 0 \qquad \tau_k > 0, \qquad g_k > 0, \qquad g_1 + g_2 + g_3 < 1 \tag{6.12}$$

The identified visco-hyperelastic material parameters are presented in Table 6.6.

| Hyperelastic parameters | $\alpha_1$ | $\alpha_2$ | $\mu_1$ | $\mu_2$ | | |
|---|---|---|---|---|---|---|
| | $-2.1990$ | 3.4435 | 0.000239 | 0.02235 | | |
| Prony-parameters | $g_1$ | $g_2$ | $g_3$ | $\tau_1$ | $\tau_2$ | $\tau_3$ |
| | 0.84226 | 0.05311 | 0.03547 | 0.16031 | 0.84929 | 1.92388 |

**Table 6.6:** The material parameters in case of closed-form parameter fitting method

Since all parameters were identified, the stability of the hyperelastic model can also be checked using the Drucker-stability criteria in Abaqus. The results of the stability analysis is presented in Table 6.7.

| Hyperelastic parameters | Stability |
|---|---|
| Uniaxial tension | Stable for all strains |
| Uniaxial compression | Stable for all strains |
| Biaxial tension | Stable for all strains |
| Biaxial compression | Stable for all strains |
| Volumetric tension | Stable for all volume ratios |
| Volumetric compression | Stable for all volume ratios |
| Simple shear | Stable for all shear strains |

**Table 6.7:** The stability of the hyperelastic model using closed-form fitting method

Therefore, we can consider our modell stable. After that, similarly to the separated method, the fitted model was validated with FEA in Abaqus. The FE model and all the settings were the same as in case of the separated fitting (see *Subsection* 6.3.3). The results are presented in Fig. 6.6. It should be remarked, that for the visco-hyperelastic material parameter there is not available any built-in fitting subroutine in Abaqus. Consequently, the form closed-form parameter fitting algorithm should be implemeneted by own codes for instance in Mathematica.

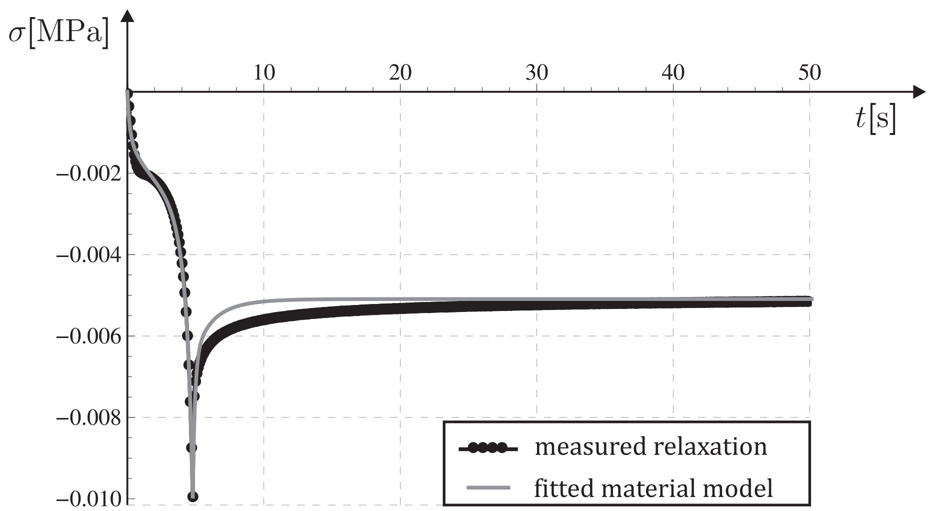


**Figure 6.6:** The results of the closed-form fitting

### 6.4.2 Predictions on the material behaviour

The identified material parameters enables us to investigate some material behaviour of the investigated memory foam material in case of further deformations and load cases. These investigation are based on the analytical formulas, that were obtained in *Chapter* 5, namely uniaxial compression and simple shear.

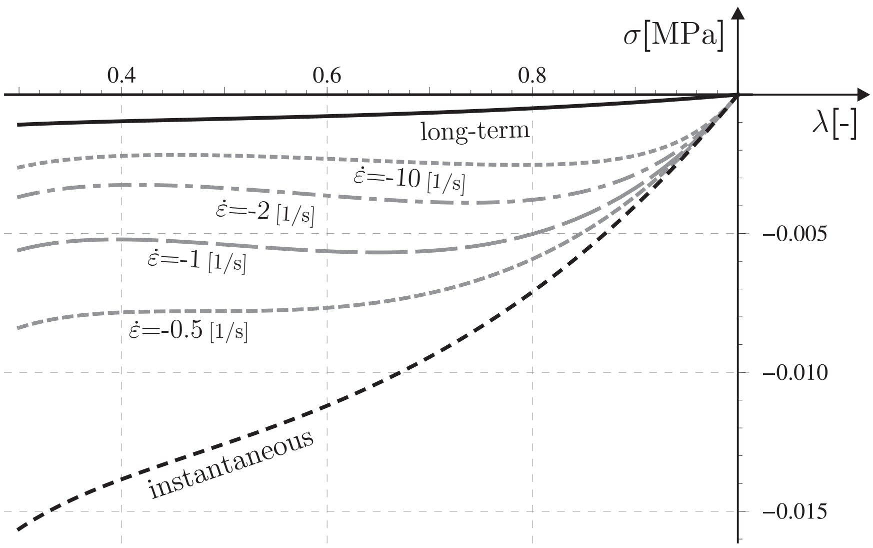


**Figure 6.7:** The stress solutions for the uniaxial uploading in case of different strain rates 1.

In case of uniaxial compression, the closed-form stress solution is obtained, thus the mechanical responses can be provided, when the speed of deformation is different for instance. Therefore the stetch input can be expressed as $\lambda(t) = 1 + \dot{\varepsilon}t$, where $\dot{\varepsilon} < 0$. In the investigations, which can also be considered as predictions, eight different strain rates are investigated including the time-independent instantaneous and long-term cases. As a result the stress-stretch characteristics were obtained, which are presented in Figs. 6.7 and 6.8.

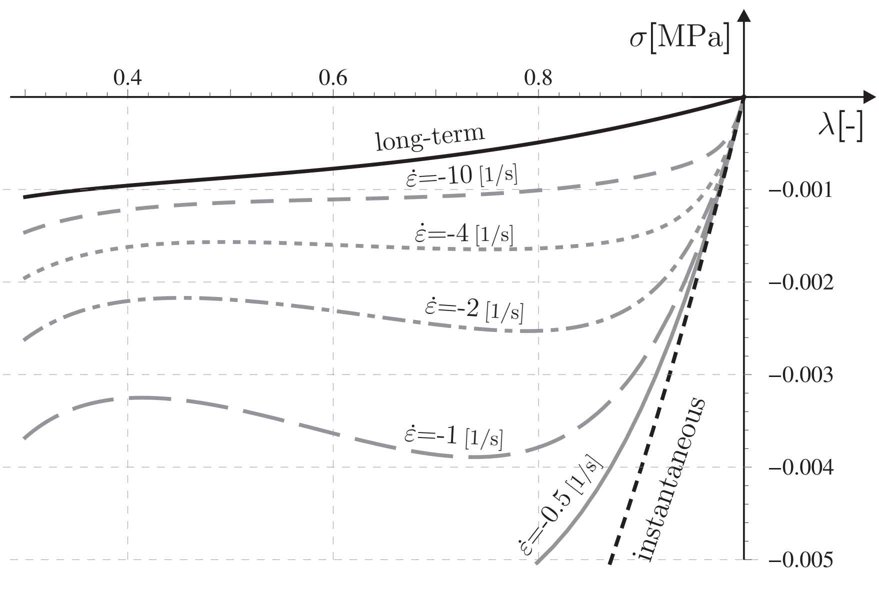


**Figure 6.8:** The stress solutions for the uniaxial uploading in case of different strain rates 2.

The results present us the effect of the strain rate during the uploading process. Additionally, it can also be seen, that the stress-stretch characteristics are always in between the long-term and the intantaneous (time-independent) characteristics.

Secondly, the simple shear case was investigated, for which the stress solution could not be solved analytically. In this case, only the instantaneous and long-term principal stress values can be calculated as it was derived in (4.18). The characteristics are presented in Fig. 6.9.

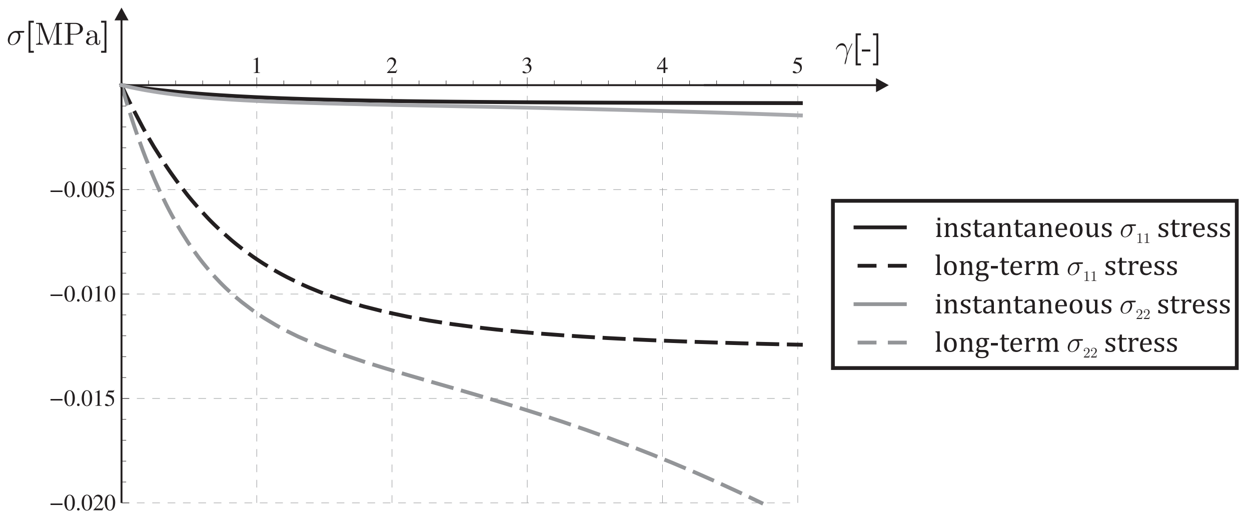


**Figure 6.9:** The principal stress caharcteristics in case of simple shear

The simple shear characteristics also gives some details about the possible time-dependent stress solutions, since the the curves should lay inbetween the long-term and the instanataneous stress responses.

## 6.5 Evaluation of results

The parameters in the visco-hyperelastic material model can be identified using two different methods: the separated and the closed form fitting methods. In the separated method the hyperelastic and the viscoelastic materials fitted in two steps using different measurement data, while the in the closed-form method the parameters are identified in one step based on the analytical solution in (4.34). The performace of the two fitting method can be compared based on the FEA analysis, where the stress relaxation measurement was investigated numerically. The comparison of the fitting methods and the measurement data are provided in Figs. (6.10) and (6.11).

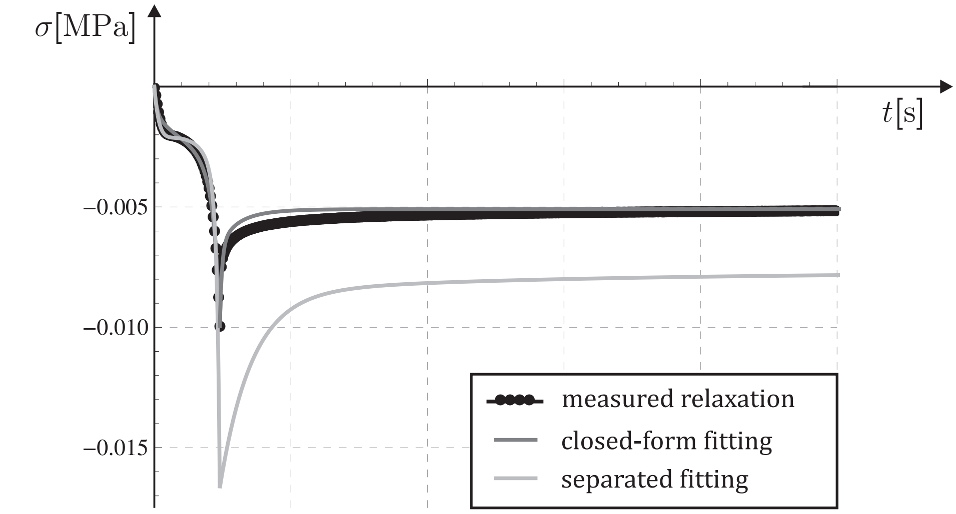


**Figure 6.10:** The comparison of the fitting methods on the $t \in [0, 100]$ interval

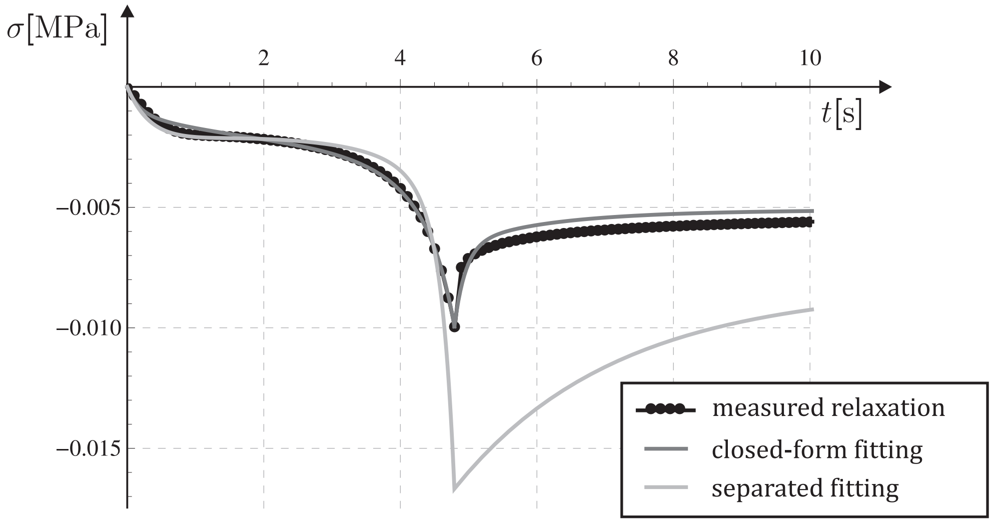


**Figure 6.11:** The comparison of the fitting methods on the $t \in [0, 10]$ interval

The figures show that the closed-form fitting method gives significantly better solution than the separated one, in which several errors were induced due to the approximations, especially in the relaxation. The difference of the methods can also be presented on Fig. 6.12, which shows the $\delta$ relative errors of the fitting methods compared to the real measurement data.

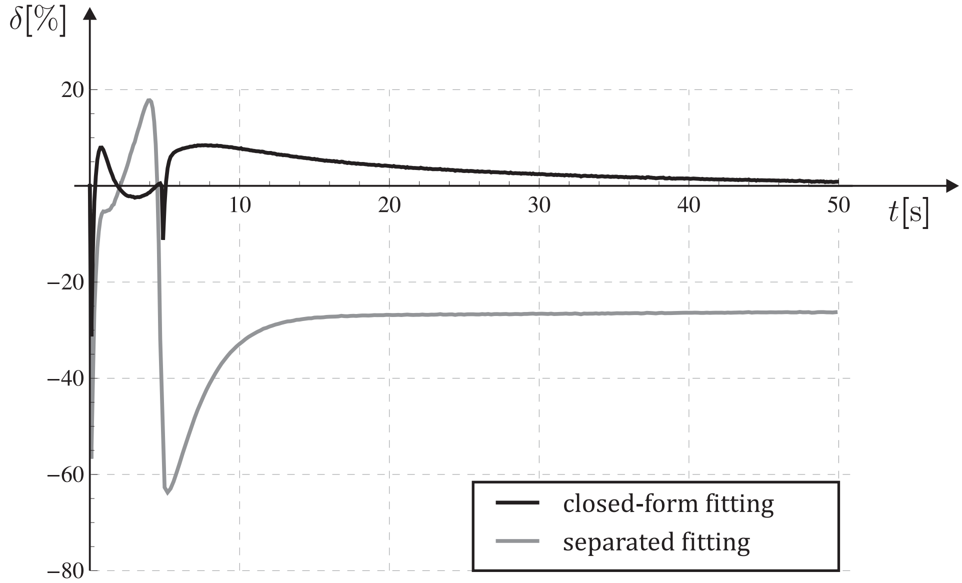


**Figure 6.12:** The relative errors of the fitting methods, compared to the measurement data

Consequently, it can be clearly seen that the closed-form fitting method improves the accuracy of the time-dependent visco-hyperelastic material model, which also improves the performance of the further numerical investigations using finite element method. Nevertheless, it should be noted, that the accuracy of the closed-form fitting process can be further improved by adopting higher order hyperelastic or Prony-series, which would also increase further the computation time during the fitting process. However, as the results show in case of uniaxial compression the second-order hyperelastic and third-order Prony-series give acceptable results and show properly the efficiency and the accuracy of the closes-form fitting method compared to the separated one.

# 7
# Summary of results

## 7.1 Summary in English

Polymer foams are widely applied cellular materials in the field of industry and in everyday use as well, due to their favourable mechanical behaviour. Therefore, there is a significant need to understand and model their mechanical behaviour properly in order to improve the finite element analysis of such materials. Since the polymer foams shows time-dependent viscoelastic properties, their mechanical behaviour can be modelled using special viscoelastic material models. Additionally, the deformation of polymer foams can be characterized by large strains and deformations, thus the linear viscoelastic modelling approach cannot be applied and the so-called visco-hyperelastic material models should be used instead. In this approach the viscoelastic material model is combined with a hyperelastic model, which describes the time-independent behaviour based on the corresponding strain energy function. The goal of my thesis was to investigate the visco-hyperelastic material modelling in case of a particular commercial memory foam material, which can be found in mattresses as well.

Firstly, I summarized the basis of hyperelasticity and introduced the Ogden–Hill's compressible hyperelastic material model and discussed its properties. This hyperelastic model is the only widely applied compressible hyperelastic model, which can characterize the behaviour of polymer foams. After that, the concept of viscoelasticity and the linear viscoelastic modelling approach were summarized, in which the time-dependent material behaviour is characterised by Prony-series. Finally, the visco-hyperelastic constitutive equation was obtained as the reformulation of the linear viscoelastic model for finite strains based on the formalism applied in Abaqus.

Since the introduced visco-hyperelastic model defines the relation of the strain history and the stress response in the form of a hereditary integral, the general stress response solution cannot be obtained. Additionally, the analytical solution of this integral has not been provided for any load case in the literature. Therefore, after summarizing the basic homogeneous deformations, I have derived the closed-form stress solution in case of uniaxial compression. This analytical solution can be directly related to the equibiaxial and volumetric compression deformations, thus the solution for these deformations are also provided.

The time-dependent mechanical behaviour of the memory foams was also investigated experimentally by uniaxial compression tests, namely relaxation and cyclic tests. The results of the measurements have shown that the behaviour of the memory foam material has viscoelastic properties, thus the visco-hyperelastic modelling approach is necessary. Besides, the compression tests also provided data for the parameter identification process.

The material parameters was identified using parameter fitting methods based on the measurement data. In my thesis two fitting approaches were applied: the separated and the closed-form methods. In the separated case the the parameter-fitting of the long-term behavior and the stress relaxation parameters are performed separately, while the closed-form solution identifies the parameters in one step. The closed-form parameter fitting method is based based on the previously derived analytical stress solution. Therefore this is a novel method, which provides a more accurate modelling approach for polymer foams. The performance of the fitted material models were analysed in Abaqus and additionally the behaviour of the fitted model was also discussed for some further loading cases as well. As a conclusion we can state that the derived closed-form solution significantly improves the material modelling of polymer foams.

To summarize the contributions, in my thesis the modelling approaches of polymer foams have been summarized and a proper visco-hyperelastic material model has been provided. Furthermore, the closed-form stress solution for uniaxial compression was derived, which was utilized successfully in the parameter fitting process.

## 7.2 Summary in Hungarian - Az eredmények összefoglalása

A polimer habok széles körben elterjedt sejtszerkezetű anyagok, amelyeket kedvező mechanikai tulajdonságaik miatt nem csak az iparban, hanem a hétköznapok során is előszeretettel alkalmaznak. Emiatt jelentős az igény arra, hogy pontos mechanikai modellt alkossunk viselkedésükről. A polimer habok mechanikai viselkedése időfüggő tulajdonságokat is mutat, emiatt speciális viszkoelasztikus anyagmodelleket kell alkalmaznunk a modellezés során. Mivel azonban a polimer habok deformációi nagy alakváltozásokkal és elmozdulásokkal járnak, ezért a mechanikai viselkedésüket a polimer habokra felírható, időfüggő viszko-hiperelasztikus anyagmodellek segítségével írhatjuk le. Azonban általános viszko-hiperelasztikus anyagmodell nem érhető el, az csak a megfelelően megválasztott időfüggetlen viselkedést leíró hiperelasztikus és a relaxációt leíró viszkoelasztikus anyagmodellek ötvözésével állítható elő. Dolgozatom célja, hogy vizsgáljam a viszko-hiperelasztikus anyagmodellezés lehetőségét a kereskedelmi forgalomban is kapható memóriahab alapanyag esetén.

Dolgozatomban először összefoglaltam az időfüggetlen hiperelasztikus anyagmodellek alapjait, valamint ismertettem a polimer habok esetén alkalmazható összenyomható Ogden–Hill-féle Hyperfoam anyagmodellt, amelyet az Abaqus végeselemes szoftverben használt formalizmus alapján írtam fel. Ezt követően követően összegeztem a viszkoelasztikus anyagi viselkedés megközelítését, a Prony-sorzatok alakjában felírható anyagmodellt, melyet először kis- majd véges alakváltozások esetén definiáltam. Az így nyert viszko-hiperelasztikus konstitutív egyenlet alkalmas az időfüggő anyagi viselkedést mutató memóriahabok leírására.

A viszko-hiperelasztikus anyagmodell esetében a feszültség és az alakváltozás közti kapcsolatot egy konvolúciós integrál segítségével lehet felírni, amely függ a bemenő elmozdulás jeltől, emiatt a feszültség válasz nem állítható elő általános alakban. Jelenleg a szakirodalomban sem érhető el a vizsgált anyagmodell zártalakú megoldása, még egyszerű terhelések esetére se. Azonban nyílt cellás habok egytengelyű terhelése esetén az anyagmodell megoldható, a levezetés lépéseit részletesen bemutatom. Mivel az egytengelyű terhelés esetén számított analitikus megoldás közvetlenül kapcsolódik a kéttengelyű illetve a térfogati összenyomáshoz, az analitikus megoldást ebben a két terhelési esetben is előállítottam.

A memória habok viselkedésének viszko-hiperelasztikus jellegét egytengelyű nyomómérések segítségével is vizsgáltam. A mérések során két tesztet végeztem el: nagy deformációsebességgel történő relaxációs mérést, valamint egy ciklikus tesztet, amely során a próbatest fokozatosan lett fel- és leterhelve. A mérési eredmények egyértelműen igazolták a memória hab alapanyag időfüggő mechanikai tulajdonságait.

A mérések alapján a felírt anyagmodellben szereplő anyagparaméterek illesztésével is foglalkoztam, melynek során két paraméterillesztési megközelítést is alkalmaztam. A szétválasztott módszer lényege, hogy a görbeillesztést az időfüggetlen (hiperelasztikus) és az időfüggő (Prony-sorozatok) anyagmodellekre külön lehet elvégezni. A zárt alakú módszer esetében az analitikus feszültség válasz függvény alapján egy lépésben illeszthető valamennyi anyagparaméter. Ez egy új paraméterillesztési eljárás polimer habok esetében, mivel a zárt alakú feszültség válasz függvény nem érhető el a szakirodalomban. Az illesztett anyagmodellek pontosságát végeselemes analízis segítségével ellenőriztem. Az eredmények alapján elmondható, hogy a zárt alakú illesztés segítségével mértékben javítható az illesztett anyagmodell pontossága, amely a későbbi végeselemes analíziseket pontosabbá és megbízhatóbbá teszi.

Összegezve, a dolgozatomban ismertettem a memória habok mechanikai modellezését, felírtam az anyagi viselkedést leíró mechanikai modellt, valamint előállítottam a zárt-alakú megoldást, amely lehetővé teszi az anyagparaméterek pontos illesztését.

# Appendix

# A

# Relation of the *Hyperfoam* material model and the Hooke's law

The parameters in the Ogden–Hill's compressible hyperelastic (*Hyperfoam*) material model cannot be chosen freely, because certain physical conditions have to be satisfied during the parameter fitting process. One of these conditions states that the linearized form of the nonlinear material model should be equal with the Hooke's law in case of small strains. The linearization is performed around the undeformed state, i.e. when $\lambda_i = 1$. Firstly, let us introduce a modified stretch-measure ($\lambda_i^*$) [25] as

$$\lambda_i^* = \lambda_i J^{-1/3}. \tag{A.1}$$

Based on this stretch-measure, the originally applied strain energy function $W(\lambda_1, \lambda_2, \lambda_3)$ can be rewritten as

$$W(\lambda_1, \lambda_2, \lambda_3) = W^*(\lambda_1^*, \lambda_2^*, \lambda_3^*, J), \tag{A.2}$$

where $\lambda_3^*$ can be expressed as the function of $\lambda_1^*$ and $\lambda_2^*$ using the relation $\lambda_3^* = (\lambda_1^* \lambda_2^*)^{-1}$. Substituting this into (A.2) the simplified strain energy function $\hat{W}^*$ becomes

$$\hat{W}^*(\lambda_1^*, \lambda_2^*, J) = W^*(\lambda_1^*, \lambda_2^*, (\lambda_1^* \lambda_2^*)^{-1}, J). \tag{A.3}$$

Based on this formulation, the initial moduli of the material model can be related to the partial derivatives of the strain energy function in (A.3), which are evaluated at the undeformed state, i.e $\lambda_1^* = 1, \lambda_2^* = 1$ and $J = 1$ [25]. Thus

$$K = \frac{\partial^2 \hat{W}^*}{\partial J^2}(1, 1, 1), \tag{A.4}$$

$$\mu_0 = \frac{\partial^2 \hat{W}^*}{\partial \lambda_1^{*2}}(1, 1, 1) = \frac{\partial^2 \hat{W}^*}{\partial \lambda_2^{*2}}(1, 1, 1) = 2\frac{\partial^2 \hat{W}^*}{\partial \lambda_1^* \partial \lambda_2^*}(1, 1, 1), \tag{A.5}$$

where $K$ is the initial bulk modulus and $\mu_0$ the initial shear modulus.

In the Ogden–Hill's hyperelastic constitutive equation according to the ABAQUS [5] formulation the corresponding strain energy function can be written as

$$W = \sum_{i=1}^{N} \frac{2\mu_i}{\alpha_i^2} \left( \lambda_1^{\alpha_i} + \lambda_2^{\alpha_i} + \lambda_3^{\alpha_i} - 3 + \frac{1}{\beta_i} \left( J^{-\alpha_i \beta_i} - 1 \right) \right), \tag{A.6}$$

which, after substituting the relations in (A.1) back, leads that the $\hat{W}^*$ function becomes

$$\hat{W}^*(\lambda_1^*, \lambda_2^*, J) = \sum_{i=1}^{N} \frac{2\mu_i}{\alpha_i^2} \left( \left(\lambda_1^* J^{1/3}\right)^{\alpha_i} + \left(\lambda_2^* J^{1/3}\right)^{\alpha_i} + \left(\frac{J^{1/3}}{\lambda_1^* \lambda_2^*}\right)^{\alpha_i} - 3 + \frac{1}{\beta_i} \left( J^{-\alpha_i \beta_i} - 1 \right) \right). \tag{A.7}$$

After expressing and evaluating the partial derivatives in (A.4) and (A.5), the initial moduli can be expressed as

$$\mu_0 = \sum_{i=1}^{N} \mu_i \tag{A.8}$$

$$K = \sum_{i=1}^{N} 2\mu_i \left( \frac{1}{3} \beta_i \right). \tag{A.9}$$

In the Hooke's law the conditions for the shear and the bulk moduli are $\mu_0 > 0$ and $K > 0$, respectively. Using the derived expressions in (A.8) and (A.9) leads that

$$\mu_0 = \sum_{i=1}^{N} \mu_i > 0, \qquad K = \sum_{i=1}^{N} 2\mu_i \left( \frac{1}{3} + \beta_i \right) > 0, \tag{A.10}$$

from which the conditions of the material parameters in the Ogden–Hill's *Hyperfoam* material model becomes

$$\sum_{i=1}^{N} \mu_i > 0, \qquad \beta_i > -\frac{1}{3} \tag{A.11}$$

It should be noted that the condition $\beta_i > -1/3$ is stricter than the necessary condition for the $\beta_i$ parameters, which significantly limits the possible domain of parameters. Although, this condition is applied in the literature and in ABAQUS as well [5].

# B
# Numerical implementation of visco-hyperelastic model

The following derivation steps follows the structure of the Theory Guide in ABAQUS [5]. Based on the definition of the visco-hyperelastic constitutive equation in ABAQUS [5], the Kirchhoff-stress solutions can be obtained as

$$\boldsymbol{\tau}^D(t) = \boldsymbol{\tau}_0^D(t) - \mathrm{SYMM}\left[\sum_{k=1}^{P}\frac{g_k}{\tau_k}\int_0^t \mathbf{F}_t^{-1}(t-s)\boldsymbol{\tau}_0^D(t-s)\mathbf{F}_t(t-s)\exp\left[\frac{-s}{\tau_k}\right]\mathrm{d}s\right], \quad \text{(B.1)}$$

$$\boldsymbol{\tau}^H(t) = \boldsymbol{\tau}_0^H(t) - \sum_{k=1}^{P}\frac{g_k}{\tau_k}\int_0^t \boldsymbol{\tau}_0^H(t-s)\exp\left[\frac{-s}{\tau_k}\right]\mathrm{d}s, \quad \text{(B.2)}$$

where $\boldsymbol{\tau}^D(t)$ is the deviatoric and $\boldsymbol{\tau}^H(t)$ the hydrostatic part of the Kirchhoff stress tensor ($\boldsymbol{\tau}$). Let us introduce the so-called internal stresses, associated with each term of the series

$$\boldsymbol{\tau}_k^D(t) = \mathrm{SYMM}\left[\frac{g_k}{\tau_k}\int_0^t \mathbf{F}_t^{-1}(t-s)\boldsymbol{\tau}_0^D(t-s)\mathbf{F}_t(t-s)\exp\left[\frac{-s}{\tau_k}\right]\mathrm{d}s\right], \quad \text{(B.3)}$$

$$\boldsymbol{\tau}_k^H(t) = \frac{g_k}{\tau_k}\int_0^t \boldsymbol{\tau}_0^H(t-s)\exp\left[\frac{-s}{\tau_k}\right]\mathrm{d}s. \quad \text{(B.4)}$$

The above introduced stresses are stored in each material point and integrated forward in time. We assume, that the stess solution at time $t$ is known and we need to define the solution at time $t+\Delta t$. The numerical integration of the convolution integrals in (B.1) and (B.2) are performed separately for the deviatoric and the hydrostatic parts.

## B.1 Integration of the hydrostatic stress

The internal hydrostatic stress values at time $t+\Delta t$ can be obtained from

$$\boldsymbol{\tau}_k^H(t+\Delta t) = \frac{g_k}{\tau_k}\int_0^{t+\Delta t} \boldsymbol{\tau}_0^H(t+\Delta t-s)\exp\left[\frac{-s}{\tau_k}\right]\mathrm{d}s. \quad \text{(B.5)}$$

Introducing $\hat{t} = s - \Delta t$ it follows that

$$\boldsymbol{\tau}_k^H(t+\Delta t) = \frac{g_k}{\tau_k}\exp\left[\frac{-\Delta t}{\tau_k}\right]\int_{-\Delta t}^{0}\boldsymbol{\tau}_0^H(t-\hat{t})\exp\left[\frac{-\hat{t}}{\tau_k}\right]\mathrm{d}\hat{t} + \exp\left[\frac{-\Delta t}{\tau_k}\right]\boldsymbol{\tau}_k^H(t) \tag{B.6}$$

To perform the integral we assume that $\boldsymbol{\tau}_0^H(t-\hat{t})$ is a linear function over the increment, therefore

$$\boldsymbol{\tau}_0^H(t-\hat{t}) = \left(1+\frac{\hat{t}}{\tau_k}\right)\boldsymbol{\tau}_0^H(t) - \frac{\hat{t}}{\tau_k}\boldsymbol{\tau}_0^H(t+\Delta t) \qquad -\Delta t \le \hat{t} \le 0. \tag{B.7}$$

Substitution back into (B.6) yields

$$\begin{aligned}\boldsymbol{\tau}_k^H(t+\Delta t) &= \frac{g_k}{\tau_k}\exp\left[\frac{-\Delta t}{\tau_k}\right]\int_{-\Delta t}^{0}\left[\left(1+\frac{\hat{t}}{\tau_k}\right)\boldsymbol{\tau}_0^H(t) - \frac{\hat{t}}{\tau_k}\boldsymbol{\tau}_0^H(t+\Delta t)\right]\exp\left[\frac{-\hat{t}}{\tau_k}\right]\mathrm{d}\hat{t} \\ &\quad + \exp\left[\frac{-\Delta t}{\tau_k}\right]\boldsymbol{\tau}_k^H(t).\end{aligned} \tag{B.8}$$

After expressing the integrals, the solution at the end of the increment becomes

$$\begin{aligned}\boldsymbol{\tau}_k^H(t+\Delta t) &= \left[1-\frac{\tau_k}{\Delta t}\left(1-\exp\left[\frac{-\Delta t}{\tau_k}\right]\right)\right]g_k\boldsymbol{\tau}_0^H(t+\Delta t) + \\ &\quad \left[\frac{\tau_k}{\Delta t}\left(1-\exp\left[\frac{-\Delta t}{\tau_k}\right]\right) - \exp\left[\frac{-\Delta t}{\tau_k}\right]\right]g_k\boldsymbol{\tau}_0^H(t) + \exp\left[\frac{-\Delta t}{\tau_k}\right]\boldsymbol{\tau}_k^H(t),\end{aligned} \tag{B.9}$$

which can be written in a simplified form as

$$\boldsymbol{\tau}_k^H(t+\Delta t) = a_i g_k\boldsymbol{\tau}_0^H(t+\Delta t) + b_i g_k\boldsymbol{\tau}_0^H(t) + c_i\boldsymbol{\tau}_k^H(t), \tag{B.10}$$

where

$$a_i = 1-\frac{\tau_k}{\Delta t}(1-c_i); \quad b_i = \frac{\tau_k}{\Delta t}(1-c_i) - c_i; \quad c_i = \exp\left[\frac{-\Delta t}{\tau_k}\right] \tag{B.11}$$

## B.2 Integration of the deviatoric stress

The internal deviatoric stress values at time $t+\Delta t$ can be obtained from

$$\boldsymbol{\tau}_k^D(t+\Delta t) = \mathrm{SYMM}\left[\frac{g_k}{\tau_k}\int_0^{t+\Delta t}\mathbf{F}_{t+\Delta t}^{-1}(t+\Delta t-s)\boldsymbol{\tau}_0^D(t+\Delta t-s)\mathbf{F}_{t+\Delta t}(t+\Delta t-s)\exp\left[\frac{-s}{\tau_k}\right]\mathrm{d}s\right]. \tag{B.12}$$

Where the push-back operator related between time $t$ and $t+\Delta t$ becomes

$$\mathbf{F}_{t+\Delta t}(t-s) = \mathbf{F}_t(t-s)\mathbf{F}_{t+\Delta t}(s). \tag{B.13}$$

Introducing $\hat{t} = s - \Delta t$, $\Delta\mathbf{F} = \mathbf{F}_t(t+\Delta t)$ and a new variable $\hat{\boldsymbol{\tau}}^D$ for which

$$\hat{\boldsymbol{\tau}}_0^D(t) = \mathrm{SYMM}\left[\Delta\mathbf{F}\boldsymbol{\tau}_0^D(t)\Delta\mathbf{F}^{-1}\right], \tag{B.14}$$

$$\hat{\boldsymbol{\tau}}_0^D(t+\Delta t) = \boldsymbol{\tau}_0^D(t+\Delta t), \tag{B.15}$$

$$\hat{\boldsymbol{\tau}}_k^D(t) = \mathrm{SYMM}\left[\Delta\mathbf{F}\boldsymbol{\tau}_k^D(t)\Delta\mathbf{F}^{-1}\right], \tag{B.16}$$

relation hold, the integral simplifies to

$$\boldsymbol{\tau}_k^D(t+\Delta t) = \frac{g_k}{\tau_k}\exp\left[\frac{-\Delta t}{\tau_k}\right]\int_{-\Delta t}^{0}\hat{\boldsymbol{\tau}}_0^D(t-\hat{t})\exp\left[\frac{-\hat{t}}{\tau_k}\right]\mathrm{d}\hat{t} + \exp\left[\frac{-\Delta t}{\tau_k}\right]\hat{\boldsymbol{\tau}}_k^D(t). \tag{B.17}$$

To perform the integral we assume that $\hat{\boldsymbol{\tau}}_0^D(t-\hat{t})$ is a linear function over the increment, therefore

$$\boldsymbol{\tau}_0^D(t-\hat{t}) = \left(1+\frac{\hat{t}}{\tau_k}\right)\hat{\boldsymbol{\tau}}_0^D(t) - \frac{\hat{t}}{\tau_k}\hat{\boldsymbol{\tau}}_0^D(t+\Delta t) \qquad -\Delta t \leq \hat{t} \leq 0. \tag{B.18}$$

Substituting back into (B.17), and performing the integration, we get exactly the same form of the stress solution as in (B.10) and (B.11), thus

$$\boldsymbol{\tau}_k^D(t+\Delta t) = a_i g_k \boldsymbol{\tau}_0^D(t+\Delta t) + b_i g_k \hat{\boldsymbol{\tau}}_0^D(t) + c_i \hat{\boldsymbol{\tau}}_k^D(t), \tag{B.19}$$

where

$$a_i = 1 - \frac{\tau_k}{\Delta t}(1-c_i); \quad b_i = \frac{\tau_k}{\Delta t}(1-c_i) - c_i; \quad c_i = \exp\left[\frac{-\Delta t}{\tau_k}\right]. \tag{B.20}$$

## B.3 Total stress solution

From the previously derived hydrostatic and deviatoric internal stress solutions in (B.10) and (B.19), respectively, the total stress at time $t + +\Delta t$ can be expressed as

$$\boldsymbol{\tau}(t+\Delta t) = \boldsymbol{\tau}_0(t-s) - \sum_{k=1}^{P}\boldsymbol{\tau}_k^D(t+\Delta t) - \sum_{k=1}^{P}\boldsymbol{\tau}_k^H(t+\Delta t) \tag{B.21}$$

which with equations (B.10) and (B.19) can also be written as

$$\begin{aligned}\boldsymbol{\tau}(t+\Delta t) \quad = \quad & \left(1-\sum_{k=1}^{P}a_i g_k\right)\boldsymbol{\tau}_0^D(t+\Delta t) + \sum_{k=1}^{P}b_i g_k \hat{\boldsymbol{\tau}}_0^D(t) + \sum_{k=1}^{P}c_i\hat{\boldsymbol{\tau}}_k^D(t) + \\ & \left(1-\sum_{k=1}^{P}a_i g_k\right)\boldsymbol{\tau}_0^H(t+\Delta t) + \sum_{k=1}^{P}b_i g_k \boldsymbol{\tau}_0^H(t) + \sum_{k=1}^{P}c_i\boldsymbol{\tau}_k^H(t),\end{aligned} \tag{B.22}$$

with

$$a_i = 1 - \frac{\tau_k}{\Delta t}(1-c_i); \quad b_i = \frac{\tau_k}{\Delta t}(1-c_i) - c_i; \quad c_i = \exp\left[\frac{-\Delta t}{\tau_k}\right]. \tag{B.23}$$

# C
# The incomplete gamma function

The following summary of the upper incomplete gamma function $\Gamma(\nu, x)$, which occurred in our calculations, is based on Spanier and Oldham: An atlas of functions [20] and the documentations provided by *Wolfram Mathword* [26], [21].

## C.1 The (complete) gamma function

The (complete) gamma function $\Gamma(n)$ is defined to be an extension of the factorial to complex and real number arguments, which is related to the factorial in case of natural numbers as

$$\Gamma(n) = (n-1)!. \tag{C.1}$$

Generally, the (complete) gamma function is defined as a definite integral for all $\mathrm{Re}(z) > 0$. A possible formulation of this function is called as Euler's integral form, in which

$$\Gamma(z) = \int_0^\infty t^{z-1} e^{-t} dt, \tag{C.2}$$

which can be alternatively given as

$$\Gamma(z) = \int_0^1 \left[\ln\left(\frac{1}{t}\right)\right]^{z-1} dt. \tag{C.3}$$

The complete gamma function can be further generalized using the so-called incomplete gamma functions, which by definition satisfy

$$\Gamma(\nu) = \Gamma(\nu, x) + \gamma(\nu, x), \tag{C.4}$$

where $\Gamma(\nu, x)$ is the so-called upper incomplete gamma function and $\gamma(\nu, x)$ the lower incomplete gamma function. The functions contain two variables: $\nu$ is called as the parameter, while $x$ is the argument in both incomplete gamma functions. The adjective "*incomplete*" reflects the restricted ranges of the definite integral compared to the complete gamma function in (C.2). The adjectives "*upper*" and "*lower*" specifies that the particular incomplete gamma function is defined on which range of the $x > 0$ domain.

## C.2 The upper incomplete gamma function

The upper incomplete gamma function is defined via an improper integral as

$$\Gamma(\nu, x) = \int_x^\infty t^{\nu-1} e^{-t} dt, \tag{C.5}$$

for all $\mathrm{Re}(\nu) > 0$ and $x > 0$. Using the above introduced notation, the (complete) gamma function $\Gamma(\nu)$ can be related to the upper incomplete gamma function as

$$\Gamma(\nu) = \Gamma(\nu, 0). \tag{C.6}$$

When the parameter $(\nu)$ is a natural number, then the function can also be expressed using the exponential sum as

$$\Gamma(n, x) = (n-1)! e^{-x} \sum_{k=0}^{n-1} \frac{x^k}{k!}. \tag{C.7}$$

The definition of the function in (C.5) can be extended to $\mathrm{Re}(z) < 0$ by utilizing the recursion formula. Therefore

$$\Gamma(\nu, x) = \frac{x^\nu e^{-x}}{\Gamma(1-\nu)} \int_0^\infty \frac{t^{-\nu} e^{-t}}{t+x} dt. \tag{C.8}$$

## C.3 Special cases

For some special values of $\nu$ and $x$, the upper incomplete gamma function reduces to other well-known functions, like

$$\Gamma\left(\frac{1}{2}, x\right) = \sqrt{\pi}\,\mathrm{erfc}\left(\sqrt{x}\right), \tag{C.9}$$

where $\mathrm{erfc}(x)$ denotes the *complementer Gauss error* function, or

$$\Gamma(0, x) = \left\{ \begin{array}{cl} -\mathrm{Ei}(-x) - i\pi, & \text{ha } x < 0 \\ -\mathrm{Ei}(-x), & \text{ha } x > 0 \end{array} \right\}. \tag{C.10}$$

where $\mathrm{Ei}(x)$ is the so-called *exponential integral* function. Furthermore

$$\Gamma(\nu + 1, x) = \nu \Gamma(\nu, x) + x^\nu e^{-x}. \tag{C.11}$$

# Bibliography


[1] M. Ashby, H. Shercliff, and D. Cebon. *Materials: Engineering, Science, Processing and Design*. Butterworth-Heinemann, 2007.

[2] G. Silber and C. Then. *Preventive Biomechanics*. Springer, 2013.

[3] N. Mills. *Polymer foam handbook: Engineering and Biomechanics Applications and Design Guide*. Butterworth-Heinemann, 2006.

[4] Wikipedia. Memory foam
Downloaded: 2015. 10. 21.

[5] Dassault Systèmes. Abaqus, version 6.14-2. 2015.
**URL**: *www.3ds.com/products-services/simulia/products/abaqus/*.

[6] S. Lee and W.G. Knauss. A note on the determination of relaxation and creep data from ramp tests. *Mechanics of Time-Dependent Materials*, (4):1–7, 2000.

[7] W.G. Knauss, I. Emri, and H. Lu. *Handbook of Experimental Solid Mechanics: Mechanics of Polymers - Viscoelasticity*. Springer, 2008.

[8] S.M. Goh, M.N. Charalambides, and J.G.Williams. Determination of the constitutive constants of non-linear viscoelastic materials. *Mechanics of Time-Dependent Materials*, (8):255–268, 2004.

[9] A. Kossa and Sz. Berezvai. Visco-hyperelastic characterization of polymeric foam materials. In *32nd International Danubia-Adria Symposium on Advances in Experimental Mechanics. Slovakia*, 2015.

[10] A. Kossa and Sz. Berezvai. Visco-hyperelastic characterization of polymeric foam materials. *MaterialsToday: Proceedings*, (Submitted), 2015.

[11] I. Dorghi. *Mechanics of Deformable Solids*. Springer, 2000.

[12] A. F. Bower. *Applied mechanics of solids*. CRC Press, 2010.

[13] EA. de Souza Neto, D. Peric, and DRJ. Owen. *Computational methods for plasticity: theory and application*. John Wiley & Sons Ltd., 2008.

[14] ANSYS Inc. Ansys mechanical, version 13.5, 2015
**URL**: *www.ansys.com*.

[15] MSC Softwares. Marc, 2015
**URL**: *www.mscsoftware.com/product/marc*.

[16] R. W. Ogden. Large deformation isotropic elasticity: On the correlation of theory and experiment for compressible rubberlike solids. *Proceedings of the Royal Society of London, Series A, Mathematical and Physical Sciences*, (328):567–583, 1972.

[17] R. Hill. Aspects of invariance in solid mechanics. *Advances in Applied Mechanics*, (18):1–78, 1978.

[18] B. Storakers. On material representation and constitutive branching in finite compressible elasticity. *Journal of the Mechanics and Physics of Solids*, (34):125–145, 1986.

[19] S. P. C. Marques and G. J. Creus. *Computational Viscoelasticity*. Springer, 2012.

[20] J. Spanier and K.B. Oldham. *An atlas of functions*. Springer, 1987.

[21] Wolfram. Mathword: Incomplete gamma function
**URL**: *mathworld.wolfram.com/IncompleteGammaFunction.html*.

[22] International Organization for Standardization (ISO) EN ISO 3386-1. Polymeric materials, cellular flexible - determination of stres-strain characteristic in compression - part 1: Low-density meaterials, 1986.

[23] Wolfram. Mathematica, version 9.0
**URL**: *www.wolfram.com/mathematica*.

[24] L.J. Zapas and J.C. Phillips. Simple shearing flows in polyisobutylene solutions. *Journal of Research of the National Bureau of Standards*, 75(1), 33-41 1971.

[25] R. W. Ogden. Elastic deformations of rubberlike solids. *Mechanics of Solids. The Rodney Hill 60th Anniversary Volume*, pages 499–537, 1982.

[26] Wolfram. Mathword: Gamma function
**URL**: *mathworld.wolfram.com/GammaFunction.html*.